Summer 2015

Characterization of T1rho sensitivity to metabolite and temperature changes

Nana Owusu
University of Iowa

CHARACTERIZATION OF T1RHO SENSITIVITY TO METABOLIC AND TEMPERATURE CHANGES

by

Nana Owusu

A thesis submitted in partial fulfillment
of the requirements for the Master of
Science degree in Biomedical Engineering
in the Graduate College of
The University of Iowa

August 2015

Thesis Supervisor: Associate Professor Vincent A. Magnotta

Graduate College
The University of Iowa
Iowa City, Iowa

CERTIFICATE OF APPROVAL

_____

MASTER'S THESIS

_____

This is to certify that the Master's thesis of

Nana Owusu

has been approved by the Examining Committee
for the thesis requirement for the Master of Science
degree in Biomedical Engineering at the August 2015 graduation.

Thesis Committee: _____
Vincent A. Magnotta, Thesis Supervisor

_____
Joseph M. Reinhardt

_____
Edwin Dove

_____
Mathews Jacob

_____
Daniel Thedens

To my family

ACKNOWLEDGMENTS

I would like to first and foremost thank the heavenly Father, without whose grace and guidance, I would not have completed this stage of my education. To my advisor, Dr. Magnotta, I give my sincerest thanks for his guidance throughout this project and for giving me the opportunity to work on such an interesting project. Also, for additional guidance, encouragement and tutelage through this laborious yet enjoyable learning process, I thank Dr. Casey Johnson.

In the beginning of this project, Marla Kleingartner and Autumn Craig, were patient in their instruction when learning to scan phantoms. For that, I say thank you, but also for the merriment you provide to lighten the environment of the lab. It makes coming to work a pleasant experience. During the interpretation of results, Dr. William Kearney was helpful and also insightful in how to follow-up with other experiments. Thank you Bill. My fellow lab members: Merry, Andrew, Cam, and Dr. Thedens, I thank for the encouragement and critique throughout this process. Lastly, I would also like to thank my family that was steadfast in their exhortation, which helped me persevere.

ABSTRACT

Spin-lattice relaxation in the rotating frame (T1ρ) is a relaxation parameter measured in nuclear magnetic resonance studies. This parameter has been found to be sensitive to chemical exchange processes occurring in diseased tissue associated with abnormal metabolism when measured in magnetic resonance imaging (MRI). Metabolic changes in tissue affected by abnormal metabolism can be quantified with good spatial and temporal resolution using T1ρ, better than a similar method of assessment known as CEST and current methods such as spectroscopic (^{1}H- and ^{31}P-MRS) and nuclear medicine (PET) methods used in clinical settings. Though T1ρ has these advantages, there is no consensus as to which metabolic changes T1ρ is most sensitive. The metabolic changes may be pH related, or due to changes in concentration of metabolites like glucose and glycogen. This work is tries to identify which metabolite evokes the greatest change in T1ρ by studying the response of three spin relaxation measures (T1ρ, T2 and T1) at different temperatures. It was found that T1ρ is more sensitive to pH changes than glucose and lysine at 3T. Also at body temperature, the pH results showed a non-linear trend for T1ρ signifying the limited range of sensitivity in the pH range of 6.9 to 7.5. The T2 results can be used to explain this trend.

PUBLIC ABSTRACT

Diseases such as Huntington's disorder, Bipolar disorder I, cancer and epilepsy have a common factor of abnormal metabolism linking them. The abnormal metabolism can alter the molecular composition of functioning tissue and cause the tissue to no longer function as it would. Clinical assessment of such diseases is usually done either with proton or phosphorus spectroscopy as well as positron emission tomography (PET). Each of these assessment tools has their advantages but their disadvantages need to be overcome to gain better image quality and minimize possible adverse effects. Recent imaging tools developed assess the abnormal metabolism by measuring certain quantities in the interaction of protons in aqueous environments. One of these tools is T1ρ and it provides some advantages over currently used imaging tools. There are questions as to what T1ρ is measuring in biological tissue and my work tries to address those questions. It was found that T1ρ is more sensitive to pH changes than glucose and lysine at 3T. Also at body temperature, the pH results showed a non-linear trend for T1ρ signifying the limited range of sensitivity in the pH range of 6.9 to 7.5. The T2 results can be used to explain this trend.

TABLE OF CONTENTS

LIST OF TABLES

LIST OF FIGURES

INTRODUCTION

Motivation

Detection of abnormal metabolism may provide new understanding and improve clinical management of neurodegenerative diseases, psychiatric disorders, cancer, and stroke. In many of these diseases, metabolic changes are thought to precede irreversible cellular damage. Therefore, detection of metabolic changes may provide an early marker of disease progression and a means to assess treatment efficacy when the disease is still potentially reversible. For example: metabolic abnormalities have been found in Huntington's disease years before onset of neurodegeneration or clinical symptoms[1]; mitochondrial dysfunction has been hypothesized to be a driver of bipolar disorder[2]; and acidosis (reduced pH) accompanying cerebral ischemia is known to precede tissue necrosis in stroke[3]. Abnormal metabolism may also directly influence behavior in psychiatric disorders. For example, abnormal pH buffering capacity, which may be caused by metabolic processes, is a significant factor in panic disorder[4]. Imaging techniques sensitive to metabolism may thus provide new insight into such diseases and a means to assess treatments. Detection of metabolic changes may also be useful to assess the response of cancer to chemotherapy and radiation treatment. A metabolic response in tumors is thought to precede volumetric changes [5] and may thus be potentially leveraged as an early indicator of treatment efficacy. In order to advance the study and utility of metabolic abnormalities in brain diseases, new tools are needed to assess these abnormalities in patients.

Current Tools

Current tools to measure metabolism are limited in many ways. Such limits affect the availability and adaptation of the tool like with magnetic resonance (MR) spectroscopy (MRS) and positron-emission tomography (PET). The repeatability of a study due to adverse effects on subjects must be considered with PET. Despite the

challenges these non-invasive tools introduce, they are still utilized clinically due to the advantages they each have.

MR spectroscopy informs on the molecular make-up in a region of interest via signal from atoms visible in a nuclear magnetic resonance (NMR) spectrum. By probing a range of resonance frequencies including that of these atoms, a plot of signal intensity is generated with respect to the frequencies applied (spectrum). Atoms visible in a NMR spectrum include hydrogen, phosphorus, carbon, fluorine and sodium. Of the atoms mentioned, hydrogen (^{1}H) and phosphorus (^{31}P) are more utilized in assessment of metabolic changes. Due to the abundance of hydrogen, ^{1}H-MRS has relatively high sensitivity when compared with phosphorus[6]. This sensitivity allows ^{1}H-spectroscopy to estimate metabolite concentrations using absolute quantification techniques. These metabolites include PCr, Cr, as well as lactate, myo-inositol, choline, glutamate, and N-acetyl aspartate[7]. Acquisition time for ^{1}H-MRS (and all forms of MRS) is long (>5min per voxel). This is because the amount of signal from solutes of interest is much lower than that of noise during acquisition, thus an average of many acquisitions must be used to minimize the effect of noise on quantifying solute signal. Also, its spatial resolution is poor (~8cm^{3} per voxel)[8] relative to the millimeter resolution of some MR techniques. Lastly, long acquisitions make whole-brain acquisition impractical in clinical settings[8].

The involvement of phosphorus in metabolism – generation and utilization of adenosine triphosphate (ATP) – provides ^{31}P-spectroscopy the means to detect changes in concentrations of inorganic phosphate (P_i), adenosine diphosphate (ADP), phosphocreatine (PCr) and ATP, among others. ^{31}P-MRS is the gold standard to noninvasively measure pH in the brain; pH can be measured because of the chemical-shift dependence between P_i and PCr[9]. Though ^{31}P-spectroscopy is specific to various metabolites, specialized equipment is required for the MR system[10], spectral information cannot be retrieved from the whole brain, spatial resolution is poor (60-100

cm^3 per voxel), acquisition time is long and its sensitivity is low (7% of MR sensitivity to hydrogen)[8].

Positron emission tomography is a form of medical imaging that uses radiolabeled (radiotracer) molecules to study the physiologic function of diseased tissue. The subject's body emits gamma photons once an electron in the body annihilates a positron from the radioactive molecule. The photons in the region of interest are then collected and used to form an image via the imager. PET can measure relative oxygen consumption rates, cerebral blood flow, and the extraction fraction of oxygen in the body, using appropriate radiotracers[7]. Radiotracers are designed to give insight into physiologic functions making PET specific and sensitive to such functions. Tracers like fluorodeoxyglucose ([^{18}F]FDG) are used to study energy consumption, while fluoromisonidazole ([^{18}F]FMISO) is employed in studying oxygen consumption[11]. Though PET radiotracers are specific and sensitive to physiologic signals there are some undesirable aspects. These include: the need a cyclotron to produce some of the tracers, poor spatial resolution[12], time needed for perfusion in the region of interest and the use of ionizing radiation.

As is evident, new imaging techniques are needed to overcome these limitations. It would be advantageous to have an imaging technique that could image the entire brain with higher spatial resolution (e.g. < 5mm isotropic) within a reasonable scan time (< 10 min) and pose no adverse effects. These advances would be beneficial because there are clinical applications where earlier diagnoses (e.g. stroke) could provide earlier intervention with preventative medication. Subjects would also benefit from having a recurrent illness assessed by such tools without exposure to ionizing radiation.

New Tools

Imaging techniques based on chemical exchange have potential advantages when compared to current tools. Chemical exchange is one of the ways molecules in

aqueous solutions interact with each other. There are many more ways of interaction, but those that are of interest in these new techniques are scalar coupling and dipole-dipole interactions[13]. The exchange interaction is catalyzed by either acid or base (*i.e.* pH)[14]. Chemical exchange interaction entails the exchange of protons H^+ between water molecules (solution) and molecules with hydroxyl (–OH), amide (–NH), and amine (–NH_2) groups (solutes). Protons from sites of exchange, one on the water and another on a functional group, move between the two species. Molecules with the functional groups of interest may include metabolites like glucose, nucleotides and lysine as well as proteins. Imaging techniques sensitive to chemical exchange processes measure the rate of exchange of protons but there are factors that affect the proton exchange rate. These include temperature as well as chemical and magnetic environment of the system. Chemical environment refers to the atoms or molecules around the exchange site and magnetic environment to the strength of magnetic field produced by the main magnet or the radiofrequency (RF) waves. Magnetic environment also concerns the magnetic susceptibility of the material placed in the field. Rates of exchange for amide group protons probed for chemical exchange is in the range of 10-30s^{-1} and those of hydroxyl groups are within 500-10,000s^{-1}, much faster in speed. Amine group protons also exchange quickly (500-10,000s^{-1})[15]. Chemical exchange is of interest because of the link between pH and metabolism as well as the potential sensitivity to the metabolites themselves.

Magnetic resonance imaging (MRI) provides two techniques based on chemical exchange: chemical exchange saturation transfer (CEST) and spin-lattice relaxation in the rotating frame (T1ρ). Advantages over current methods include the use of non-ionizing radiation, short acquisition time and spatial resolution. Though, the form radiation subjects are exposed is low in energy, subjects can experience heating due to the irradiation. There are rules enforced by the FDA to limit the heating of tissue

exposed to radiofrequency radiation, these are known as specific absorption rate (SAR) limits. In MRI, innate properties of tissue provide the contrast seen in images. These properties include molecules that have the aforementioned functional groups attached. Some of those molecules have a specific link to abnormal metabolism and are known as endogenous contrast agents (utilized in CEST). Another property useful to MRI is the structural makeup of different types of tissue; different types of tissue show different relaxation behavior. Relaxation refers to measurement of magnetization signal as nuclear magnetic moment vectors (spins) of atoms are manipulated by irradiation of radiofrequency waves. The spins of atoms made to align parallel or antiparallel with the static magnetic field and signal is received from them in the course of image acquisition and used to form images.

CEST

CEST images are acquired by first applying a saturation pulse for a long duration; saturation is irradiation that equalizes the population of parallel and antiparallel magnetization among the magnetic moments of solute protons. The net magnetization of the region of interest is then zero but zero magnetization is not accomplished in real situations because true equalization takes too long ($>5T_1$)[15]. As the saturation pulse is applied at a set of frequencies matching resonance frequencies of protons of the solute populations, proton exchange continues. In this set, there are symmetric offset frequencies from the resonant frequency of interest. The transfer of saturated protons onto water exchange sites decreases the net magnetization signal of water molecules. Water signal loss is amplified as the saturation pulse is on because unsaturated protons become saturated as they are transferred to solute exchange sites, further decreasing water signal. To quantify the contribution of proton exchange, a Z-spectrum is generated using the signal resulting from the irradiation process. The Z-spectrum is a plot of the decreased water magnetization signal as a function of the irradiation

frequencies divided by the magnetization without saturation (normalizes signal). Proton exchange contribution can be determined by subtracting the normalized signal at the left offset frequency from that on the right, producing a magnetization asymmetry curve. With the asymmetry curve, contributions from specific metabolites can be discerned.

Advantages of CEST have been shown through these specific metabolites that include the pertinent functional groups (-NH, -NH_2, -OH) in their composition but there are also disadvantages. CEST is sensitive to many such metabolites *in vivo*; creatine, myo-inositol and amide protons of proteins and peptides are among a list of metabolites that have been investigated with CEST[16]. Amide proton transfer (APT)[17,18] has been used to detect metabolic and pH changes in tumors, stroke and other pathologies linked to abnormal metabolism. Hydroxyl group protons of myo-inositol (MICEST)[19] may be biomarkers for various neurologic disorders. Amine protons of creatine (CrCEST)[20] might be useful in diagnosing cardiac and skeletal muscle disorders. Though CEST is specific to certain metabolites, imaging the fast exchange of hydroxyl and amine groups at clinical field strengths ($B_0 \leq 3T$) is not optimal because of the insufficient chemical difference provided. An exchange criterion set for CEST requires the chemical shift difference of water and solute protons to be greater than or equal to the observed exchange rate ($k_{ex} \leq \Delta\omega$); $\Delta\omega$ increases linearly with field strength, so stronger static fields can optimally detect faster exchanging protons[16]. An additional disadvantage of CEST is the effect of the saturation scheme on acquisition time. It can lengthen the scan time of an imaging session depending on the number of frequencies being probed. Additionally, the contributions of magnetization transfer and direct saturation increases with saturation time, making it harder to distinguish from that of proton transfer.

Since the saturation scheme can make it difficult to get reasonable scan time, a different method of imaging metabolic abnormalities is needed. T1ρ or spin-lattice

relaxation time in the rotating frame is a method that can image faster and with higher temporal resolution than CEST.

T1ρ

Spin-lattice relaxation in the rotating frame (T1ρ) is a relaxation time constant measured as the MR signal is sensitized to water protons participating in chemical exchange processes. The motion of protons during chemical exchange occurs at low frequencies and the spin-lock pulse utilized in T1ρ measurement allows the relaxation to be measured. This spin-lock RF pulse produces a low strength magnetic field (B_1<2mT)[21] which oscillates at frequencies matching that of the exchange processes and thus is sensitive to those processes. While the protons are in the weak-locking field, the stronger static field provides a means for sufficient detection (sufficient signal-to-noise ratio) by aligning more of the solute proton spins parallel to its field lines. Increase in the number of parallel spins leads to higher signal. The reason being, spins aligned with the field are lower in energy than those that are antiparallel and once energized with RF radiation, signal is produced.

Signal from the relaxing spins decays exponentially with a decay constant T1ρ governed by the Equation 1.1, where TSL is the duration of the spin-lock pulse. The decay constant can be quantified by collecting multiple signal samples with varying spin-lock durations and then fitting them to the linear model below (Equation 1.2).

$$S_{TSL} = S_o e^{-TSL/T_{1\rho}} \tag{1.1}$$

$$T_{1\rho} = -TSL/\ln\left({}^{S_{TSL}}/_{S_0}\right) \tag{1.2}$$

The signal measured is generated in magnetization preparation, which occurs before image acquisition. Preparation begins with the tipping of spins with a 90° excitation pule and immediately after that, a spin-lock RF pulse is applied parallel to the

orientation of the spins. Following the spin-lock pulse, another 90° excitation pulse is played in the opposite x-direction to realign the spins with the static magnetic field.

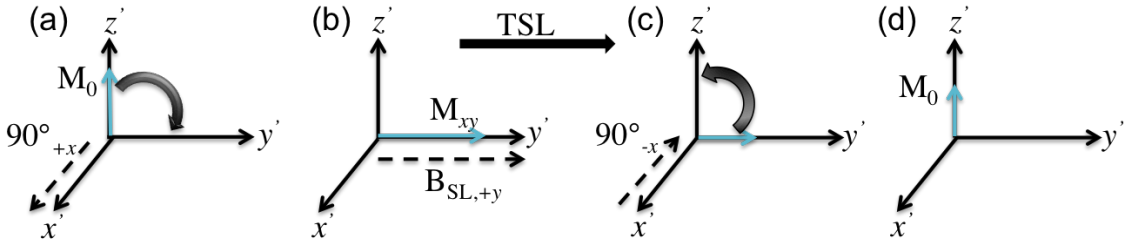

Figure 1.1: Illustrated here are a net magnetization vector and the three-dimensional space in which it exists. M_0 is the initial net magnetization vector, M_{xy} stands for transverse magnetization, TSL is the spin-lock duration and B_{SL} is the amplitude of the spin-lock pulse. There are four panes to depict the orientation of the spin as RF pulses are applied to prepare the magnetization for T1ρ. In (a) a 90° excitation pulse is applied in the x-direction which causes the spin to rotate onto the x'y'-plane, (b). A spin-lock pulse is then applied parallel to the orientation of the spin. For the time in which the locking field is applied, the net magnetization vector (*i.e.* the detectable signal) decays with time constant T1ρ, (c). Another 90° excitation pulse is applied in the opposite direction of the initial excitation, bringing the spin to its initial orientation. From here, (d), the spin is said to be T1ρ prepared.

This scheme is portrayed in Figure 1. With this realignment the magnetization is said to be T1ρ prepared and the scanner sensitive to the exchange of solute and solution protons. Factors contributing to T1ρ signal *in vivo* include pH, glucose, and other metabolites as well as temperature, static and RF magnetic fields. Of the factors pertaining to chemical exchange (pH, metabolites, and temperature), it is not clear which evokes the greatest response in T1ρ. This research project tries to define which of these factors achieve the greatest response from T1ρ.

In the measurement of T1ρ relaxation, 90° excitation pulses can be applied quickly (continuous wave) or slowly (adiabatic). There are advantages and disadvantages to both, primarily affecting energy deposition and spin uniformity (B_1-sensitivity). Continuous wave excitation pulses have lower energy deposition compared to the adiabatic, but they have higher sensitivity to B_1-inhomogeneity. This may cause non-uniform tipping of spins. However, the slow energy deposition of adiabatic pulses allows

for uniform tipping of spins, leading to better estimation of the relaxation time. Adiabatic excitation pulses deposit energy more slowly and uniformly, thus are prone to exceeding the specific absorption limits of human imaging. The spin-lock pulse has a frequency of ω_1 ($\omega_1=\gamma B_1$) that causes the relaxation time to increase as the strength of the spin-lock field is increased. Relaxation studies where spin-lock frequency is varied, known as dispersion, can be useful in determining the contribution from exchange between two chemically shifted nuclei[13]. Deposition of RF energy is dependent on the frequency of the pulse and the duration of the applied pulse, this limits the amplitude and length of the applied spin-lock pulse in human studies. Due to speculations that pathologic states of tissue can affect chemical exchange processes, T1ρ has been applied to various illnesses associated with altered chemical exchange processes. Also, T1ρ can image these exchange processes in shorter acquisition time (<5min)[22] and better spatial and temporal resolution than CEST.

Sensitivity of T1ρ to chemical exchange processes is the reason T1ρ is utilized in assessment such illnesses. This sensitivity is also provides the quantitative aspect of T1ρ which is utilized in quantitative imaging studies. Quantitative imaging studies aim to characterize mechanisms in pathological processes using quantitative measures of relaxation, proton density and diffusion coefficients. Apart from T1ρ, there are other forms of relaxation measured in MRI and these include spin-lattice relaxation (T1) and spin-spin relaxation (T2). In T1 relaxation, the exchange of energy between water protons and protons of surrounding macromolecules is measured. For T2, it is the dephasing of water proton spins due to interaction with one another that is measured. T1ρ in quantitative imaging studies have provided insight into some neurodegenerative diseases/disorders, and led to promising results in detection of various neurological diseases. These diseases include cancer Alzheimer's disease (AD), Parkinson's disease (PD), Huntington's disease (HD) and epilepsy. The following are examples of quantitative

imaging findings with T1ρ. In euthymic participants with bipolar I disorder, elevated T1ρ values in the cerebellum provided more evidence as to why the cerebellum should be appreciated as a region of interest in the disease progression[22]. Work by Wassef *et al*. has shown the striata of pre-manifest Huntington's disease subjects to have increase in T1ρ values, which is consistent with the decrease in glucose metabolism found in that region by other researchers[23]. To differentiate AD from demented and non-demented PD patients as well as healthy human controls, Haris *et al*. use T1ρ due to the changes in macromolecular composition associated with both diseases[24]. Results showed elevated T1ρ values when comparing values from right and left hemispheres of AD to that of controls. However the same regions showed decreased values in comparison of PD to controls. Elevated T1ρ values have been shown 18 hours after chemotherapy treatment in mouse model with cancer[25]. This study showed that the metabolic response of tumors due to chemotherapy treatments could be detected earlier with T1ρ than with T2. Lastly, in efforts to predict persons susceptible to epileptic seizures, traumatic brain injuries were induced in rats. 12 months after the insult, the greatest predictive value for seizure susceptibility was found with T1ρ values measured 9 and 23 days post injury, at [26]. The predictive value for T2 and a diffusion tensor measure (Dav) in the same time frame were found to be lower than that of T1ρ at 12 months. Seizures due to traumatic brain injuries may be linked to abnormal metabolism because of the inflammatory response to tissue damage. Inflammation is linked to increased acidity in the extracellular matrix of affected cells and could explain the utility of T1ρ imaging to study such injuries[27].

T1ρ can also be imaged functionally. Functional imaging refers to the imaging of physiologic or biochemical response of tissue to external or internal stimuli. To capture these responses, adequate temporal resolution (in the order of seconds) is needed. In the brain, factors contributing to the functional signal originate mostly from blood,

tissue, cerebrospinal fluid and changes in metabolite concentration in the volume imaged. Because the movement of blood is associated with the physiologic response in the brain, T1 and a variant of spin-spin relaxation, $T2^*$, are accounted for in the signal model[28]. The signal model can vary depending on the imaging sequence used to acquire the spin-lock images. T1 and $T2^*$ are included because gradient echo based sequence is used but with a spin-echo based sequence[29], only T1 is included. Signal due to tissue alone can be measured by suppressing blood signal. Blood signal suppression can be done by either paramagnetic metal nanoparticles[30] or application of a saturation pulse[9]. In an application of functional T1ρ to panic disorder, the visual cortex of participants showed increased values when stimulated with a flashing checkerboard[31]. Heo *et al.*[9] also showed during visual stimulation that 73% of signal from functional T1ρ signal was from tissue acidosis and 27% from cerebral blood volume at 3T. Work by Jin and Kim[30] concurs with Heo *et al*. inasmuch as cerebral blood volume signal being low in contribution to the response.

Although T1ρ has been effective in many applications, it is not clear which metabolic factors or tissue structures are driving the changes seen in T1ρ. Defining the most prominent factor(s) would be beneficial to clinicians. There would be a better understanding of what is causing the changes being seen. This could then lead to ways to treat the illness.

T1ρ Physics

Radiofrequency (RF) waves, utilized in magnetic resonance imaging to manipulate the spins of protons, are a form of electromagnetic radiation that has low energy. There are other forms of electromagnetic radiation and each form can behave like a wave with a distinct range of oscillation frequencies. The oscillating frequency of electromagnetic radiation is directly related to its energy. Equation 1.3 below shows this

relationship; here, *v* is the frequency of the wave and *h* is Planck's constant ($6.62\times10^{-34}m^2kg/s$).

$$E = h\nu \tag{1.3}$$

Electromagnetic radiation interacts with matter, which is made up of atoms. In this interaction, energy from the radiation is transferred to the atoms, causing them to be more energetic. However, the atoms retain the energy for only a short period of time before returning to their lower energy state. In magnetic resonance imaging, the magnetic field generated by RF radiation causes the spins of atoms, particularly hydrogen atoms, to tip and rotate (precession) about the external magnetic field. The signal detected in MRI is the RF radiation sent from the atoms after excitation with RF energy.

The RF excitation pulses concerned with this work are adiabatic, which means energy in a desired frequency range is being slowly swept by the RF amplifiers. It also means there is some immunity provided against non-uniform tip angles caused by inhomogeneity in the B_1-field. The slow sweep of frequencies is due to the phase changes designed into the pulse. To design adiabatic pulses, functions that allow amplitude modulation are required so that the peak amplitude can be set as not to exceed the specific absorption limits. Frequency modulation is also required for selecting the range of desired frequencies to excite and other spectral profile characteristics. Hyperbolic secant functions, amplitude and frequency modulation functions are frequently used when designing adiabatic pulses[32]. The Shinnar-Le Roux algorithm can also be used for designing adiabatic pulses[33,34]. Though adiabatic pulses are being discussed in the context of excitation pulses, the spin-lock pulse can also be adiabatic. However, the chemical exchange process observed in the adiabatic versus continuous wave spin-locks would be different.

The phenomenon being observed when a spin-lock is applied is the interaction between two disproportionate species, the solute and solvent protons. The water proton concentration (~110M) is far greater than that of solute protons (μM - mM range) *in vivo*[15]. Consider an instance of chemical exchange between a solute and solution molecule. Exchange between the two sites occurs at locations of the molecules with loosely bound hydrogen atoms (exchangeable protons). Also, at both sites, there is a distinct magnetic environment and a distinct Larmor frequency. Using the Bloch-McConnell equations, a mathematical expression for the spin-lattice relaxation rate (1/T1ρ) of the two-site exchange is derived[13].

$$\frac{1}{T_{1\rho}} = \frac{1}{T_{2,0}} + \frac{p_a p_b \delta^2 k}{\omega_1^2 + k^2} \tag{1.4}$$

The above equation, 1.4, is the spin-lattice relaxation rate when the spin-lock is applied 90° to the initial orientation of the spins (on-resonance). It is also representative only of the unequal population of the proton species that are exchanging. In this equation, $1/T_{2,0}$ is the transverse relaxation rate due not to chemical exchange interactions; k is the sum of exchange rates of water protons (k_w) and solute protons (k_s) species ($k=k_w + k_s$), p_w and p_s are the population of exchange sites for each species ($p_w = k_w/k$; $p_s = k_s/k$). The variable ω_1 is a property of the RF magnetic field and δ is a property of the molecules with the exchange cites. The distinct Larmor frequencies ($\omega_0 = \gamma B_0$) at both sites are subtracted to give δ, which is the chemical shift difference ($\delta = \delta_w - \delta_s$). Also, the spin-locking RF pulse produces a magnetic field with frequency ω_1 (γB_1). This expression of the rotating frame of reference spin-lattice relaxation rate denotes some of the factors that affect T1ρ relaxation and thus affects its estimation *in vivo*.

Among the factors affecting T1ρ relaxation are macromolecular composition, exchange kinetics, pH, temperature, water content and the magnetic fields generated by the main magnet and RF radiation. Macromolecular composition in particular,

pertains to biological compounds found in cells of living organisms. These compounds include the proteins, nucleotides, nucleic acids, and metabolites (glucose, acids, glutamate, etc.). Sensitivity and specificity of T1ρ to changing metabolite concentrations is not well understood at clinically relevant field strengths. The same can be said of any of these compounds. However, sensitivity to some of these compounds is known for ultra high field strengths. The chemical shift difference–which is important in distinguishing solute proton signal from that of solution–is dependent on the strength of the main magnetic field, and the greater the field strength, the shorter the relaxation time. As can be shown through algebraic manipulation, the exchange rate of either species of proton is dependent on population of the other ($k_w = k_s/p_w - k_s$). Population is determined in an experiment by retrieving the concentration of both solute and solution molecules as well as the size of each population. Retrieval of such information is affected by the chemical shift difference. If the difference were large, the signals are more distinct so the population information can be ascertained. It is more difficult with a small chemical shift difference. The proton exchange rate of solute protons is used to calculate that of solvent protons. These are known from empirical findings *in vitro*. However, *in vivo*, it is difficult to distinguish signal from solute pool from solution pool. Inability to distinguish the signals *in vivo* is due to the presence of other macromolecules in the exchanging system interfering with the measurement.

Temperature, which affects the kinetics (thermodynamic property of the collision of atoms in solution) of molecules in chemical reactions, also affects the quantification of exchange rates. High temperature means more kinetic energy is transferred to the molecules, thus more collisions, which also mean faster exchange. Low temperature means the exact opposite. Kinetics of a reaction is also affected by the concentration of each species in solution. This is because there will be more collisions with higher populations. The hydrogen ion, which is a metabolite because of its

participation in metabolic cycles, greatly affects chemical exchange. Its concentration is used in the quantification of acidity, also known as pH. Increased hydrogen ion concentration leads to low pH (acidic when below 7) while decreased concentration means high pH (basic when above 7). The prevalence of hydrogen ions leads to more proton exchange, which can affect the number of negatively charged or dipolar sites[35]. Some of these sites could be available for hydrogen bonding but the high concentration hydrogen ion can weaken those bonds and disrupt that interaction between molecules. Much like hydrogen ions affect exchange rates, bases or electron donating charged groups also affect exchange rates. It has been shown that proton exchange groups adjacent to negatively charged groups on molecules have decreased exchange rates when compared with exchange groups that are farther away from the negatively charged group[36].

Some of the factors discussed here can be used to characterize the sensitivity and specificity of T1ρ. These include varying types of exchangeable protons in metabolites as well as temperature, pH and ionic charge. By isolating different types of exchanging protons, sensitivity of T1ρ to a specific molecule like glucose can be determined. Since temperature is a factor affecting chemical exchange, T1ρ and other relaxation times can be measured during exchange at different temperatures to see how they are affected by temperature. Response from temperature experiments may show the behavior of T1ρ at body temperature. The effects of negatively charged groups on proton exchange groups could be used to determine the sensitivity to charged groups with T1ρ.

T1ρ Sensitivity and Specificity

Since T1ρ signal originates from both chemical exchange and non-exchange processes, its sensitivity and specificity to a particular molecular interaction *in vivo* is difficult to determine. Non-exchange processes of the interaction of molecules in

aqueous solutions relevant to T1ρ include dipole-dipole and scalar-coupling interactions. Dipolar interactions contribute to frequency dependence (dispersion) of relaxation times in biological tissue. This may be due to the dipolar field generated from the rotation of water molecules bound to protein[13]. Scalar coupling is related to the influence of interacting magnetic fields and electric fields on the proton spins[13]. Though researchers have assessed the sensitivity and specificity of T1ρ, not many of those works have been at clinical field strengths.

Of the work that has been done at higher field strengths to characterize T1ρ, *in* vivo and *in vitro* experiment have been conducted. In imaging mouse embryos at 2 and 9.4 T, Engelhardt and Johnson showed that T1ρ values in observed tissue decreased from low field to high field[37]. The authors ascribed the static field dependence to susceptibility gradients in tissue. Hemodynamics in tissue were thought to affect T1ρ values in tissue because of blood oxygen level-dependent effect in T2[38]; T2 relaxation contributes to T1ρ as shown by Equation 1.4. However, work by Kettunen *et al*. where cerebral ischemia was induced in rats showed that intravascular susceptibility effects caused by the level of deoxyhemoglobin have negligible effects on parenchymal T1ρ signal[39]. This work by Kettunen *et al*. was conducted at 4.7 T and it was also shown that with a unit drop in pH value, parenchymal T1ρ rose by 4.5%. Sensitivity of T1ρ to metabolites containing amide, hydroxyl and amine protons has also been shown for high field strengths. For example, at 7 and 9.4T, sensitivity of T1ρ to glucose (contains hydroxyl groups) metabolism is shown. By injecting doses of glucose and 2-deoxyglucose intravenously into rats, Jin *et al*. at 9.4T show that the T1ρ response to 2-deoxy-D-glucose is approximately 2.2 times higher that that of D-glucose in the brain after 2 hours of high temporal resolution imaging[40]. This is because 2-deoxy-D-glucose cannot be fully metabolized by cells, so it accumulates, giving a strong glucose signal. At 7T, Zu

et al. also show T1ρ having more sensitivity and specificity to proton exchange between 2-deoxy-D-glucose and water molecules than CEST in test imaging objects (phantom)[41].

For amine and amide protons, imaging experiments on phantoms containing albumin (water soluble protein) have been conducted. Particularly, Jin and Kim, with T1ρ dispersion experiments show insensitivity to amide proton transfer in egg-white albumin phantoms with varying concentrations of hydrochloric acid at 9.4T[30]. The authors also show sensitivity to amine proton exchange when a constant concentration of glutamate is added to the phantom. By adding glutamate, the pH dependence of T1ρ was affected by the fast exchange of the amine group protons. These characterizations of T1ρ at high field strengths have been insightful, however knowing that T1ρ has static field dependence, it would be helpful to medicine to provide such information for clinically relevant field strengths. Sensitivity to changes in pH has been shown for T1ρ at clinical field strengths[10] but because higher field strengths provide increased sensitivity to faster exchange proton, sensitivity to protons of hydroxyl and amine groups are not known for clinically relevant field strengths.

In general, changes in pH or glucose concentrations are thought to the main factors driving the change in T1ρ observed in tissue. Kettunen *et al*.[42] reported that in their work where global ischemia induced by cardiac arrest in rats, T1ρ did not respond to increase or decrease in blood glucose levels before stroke was induced. It was however shown that after induction of ischemia, T1ρ and T2 increased immediately. This experiment was conducted at 4.7T and also gives evidence for sensitivity of T2 to pH changes since the response to ischemia was measured after injecting the rats with a blood signal suppression agent. However, in work done by Jin and Kim[30], T1ρ of brain tissue in cats being functionally imaged showed inconsistent results during induction of global ischemia and hypercapnia. The authors conclude from this that there are different mechanisms affecting T1ρ but not necessarily pH. It must be stated though

that the differences in physiologic response during either ischemia or hypercapnia may have been the cause for the inconsistency. Also, the differences in field strength must be considered when comparing the two results. Therefore to be able to state the specificity and sensitivity of T1ρ to either pH or glucose at clinical field strengths, a comparison of responses between the two must be made at the respective field strengths.

Specific Aims

The goal of this research is to characterize the sensitivity of T1ρ at 3T to these factors listed: temperature, pH, metabolite concentration (glucose and lysine), charge structure, and dispersion. By measuring multiple relaxation parameters (T1ρ, T1 and T2), complementary information provided by each parameter might speak more about the specificity of T1ρ to these factors. To help guide the characterization, four aims/goals were set. The aims and the corresponding hypotheses are listed below.

Aim 1: Determine if T1ρ is more sensitive to pH changes than T2.

Hypotheses:

- T1ρ values will increase as pH decreases.
- In pH values within and out of the physiologic range, T1ρ will be more sensitive than T2.
- T1rho will remain linear in trend at 36, 0 and 22 °C.
- T1ρ will be more responsive than T2 at all of the temperatures

Aim 2: Determine if T1ρ is more sensitive to glucose changes than T2.

Hypotheses:

- T1ρ will decrease with increasing glucose conc.
- T1ρ will be more sensitive than T2 to glucose changes
- T1ρ will remain linear in trend at 36, 0 and 22 °C.
- T1ρ will be more responsive than T2 at all of the temperatures

Aim 3: Determine if T1ρ is sensitive to lysine.

Hypotheses:

- T1ρ will decrease with increasing lysine conc.
- T1ρ will remain linear in trend at 36, 0 and 22 °C.
- T1ρ will be more responsive than T2 at all of the temperatures

Aim 4: Observe relaxation in both pH and metabolite phantoms for a dispersion effects.

Hypothesis:

T1ρ values will increase as the spin-lock frequency increases in imaging pH and glucose phantoms.

METHODS & MATERIALS

All the solutions imaged were conducted using 50mL conical tubes (Sarstedt; Nümbrecht, Germany), which were filled to 45mL with solution. The vials were placed vertically in a polyethylene cylindrical container and bathed in water to avoid the artifacts associated with RF transmittance through an air-substrate interface and to manipulate and maintain temperatures in the vials. Images were taken using a Siemens Tim Trio 3T MRI system (Siemens Healthcare; Erlangen, Germany) using a 12-channel head coil. For the quantitative T1ρ and T2 measures, a turbo spin echo sequence was used to acquire a two-dimensional coronal slice of the vials. Preparatory pulses for the quantitative measures were played before the turbo spin echo (TSE) in the imaging sequences used. These pulses included the basic adiabatic spin-lock for T1ρ (Figure 2.1) and Malcolm Levitt's version of T2 quantification with four 180° refocusing pules (MLEV-4) for T2 (Figure 2.2). The spin-lock pulses were applied + and - 90° to the initial magnetization. Quantitative T1 measures were collected with an inversion-recovery spin echo sequence (IRSE, Figure 2.3), the TSE version was used in some experiments to decrease the time of the imaging session. The duration of the preparatory pulses and specifics about the imaging sequences are provided below for each experiment conducted. Homogeneity of the static and RF magnetic fields were determined using quantitative methods (B_0 and B_1 mapping).

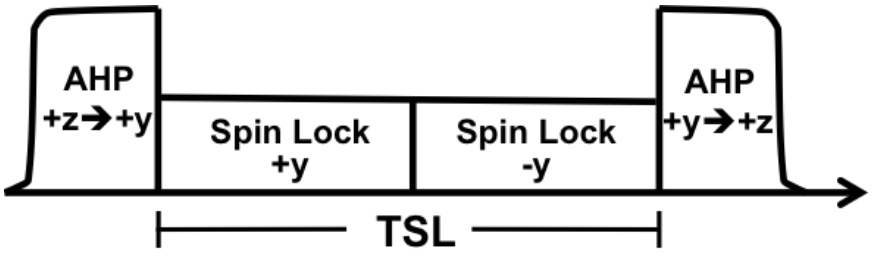

Figure 2.1: Adiabatic excitation T1ρ preparatory block. The excitation pulses here are adiabatic half passage pulses (AHP) that bring the initial longitudinal magnetization to the transverse plane. Two continuous wave spin-lock pulses are applied parallel to the transverse magnetization in succession for a time (TSL) and used to prepare the spins.

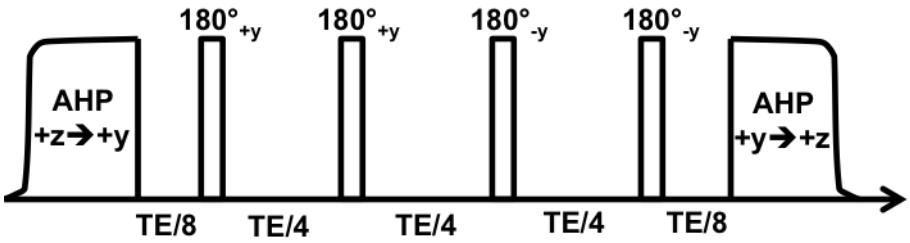

Figure 2.2: Adiabatic MLEV4 T2 preparatory block. The excitation pulses here are adiabatic half passage pulses (AHP) that bring the initial longitudinal magnetization to the transverse plane. Four 180° continuous wave pulses are used to refocus the spins in the transverse plane in time intervals dependent on a desired echo time (TE).

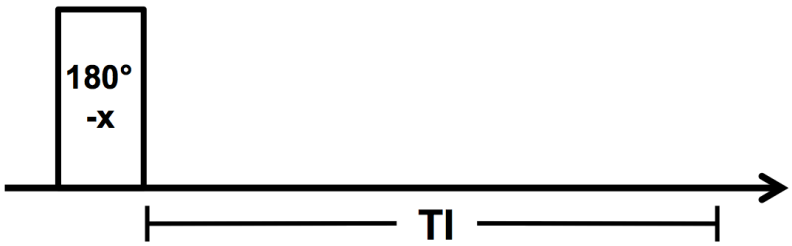

Figure 2.3: Inversion recovery preparatory block. A continuous wave 180° excitation pulse is played perpendicular to the initial magnetization, causing an inversion of the spin that would take some time (TI) to recover back to the original orientation.

Estimation of the relaxation times from the acquired images was performed voxel by voxel basis using MATLAB. For T1ρ and T2 estimation, images acquired at different TSLs or TEs were fit to Equation 1.4 to fit for the relaxation time. T1 values were calculated by fitting IRSE images acquired with different inversion times to Equation 2.1.

$$S_{TI} = S_0(1 - 2e^{-TI/T1}) \quad (2.1)$$

These fitting routines were performed on every voxel of the image, yielding T1ρ, T2 and T1 quantitative maps of the phantom vials. The median value of quantitative values in a circular region of interest, as well as the standard deviation, was recorded for each vial. Figure 2.4 shows a typically drawn region of interest. If artifacts were present, the ROI was defined to avoid regions with large variations in B_0 and B_1 based on acquired maps.

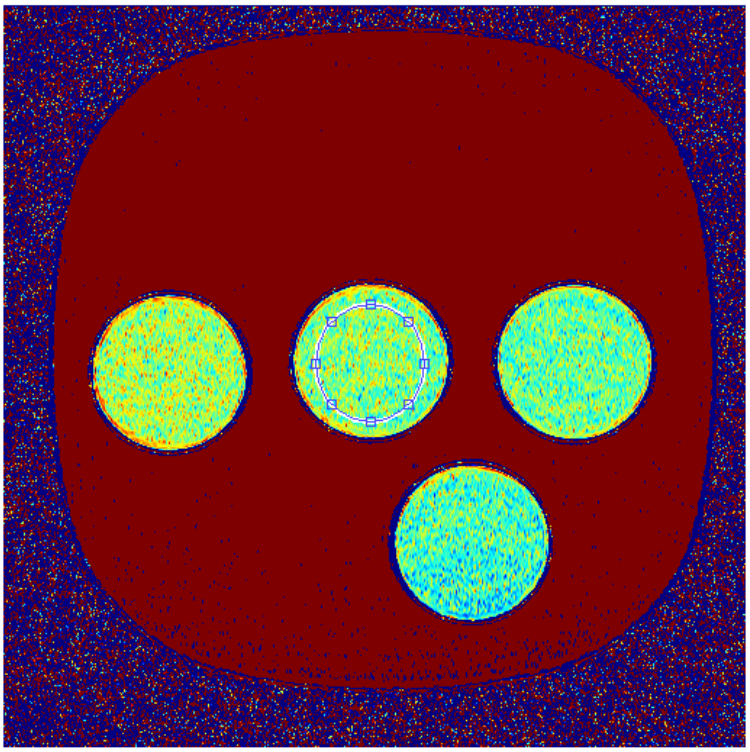

Figure 2.4: Typically drawn region of interest

Next, a plot of the quantitative relaxometry values for each vial was generated using these ROI measurements. Relative change in the relaxation times in the vials was calculated. Such plots were generated with respect to the lowest concentration of glucose or lysine and neutral pH 7. Error propagation was used to translate the standard deviation at each vial unto the relative change plot. Initially, error for the difference operation is propagated with the equation below.

$$\sigma_C = \sqrt{(a\sigma_A)^2 + (b\sigma_B)^2}$$

Where σ_A is the standard deviation at a certain vial, σ_B the standard deviation at the reference vial, and *a* and *b* are constants. The relative change calculation produces a percentage so the result is multiplied by 100, thus *a* = *b* = 100. The result of this calculation is used in propagating the division operation error.

$$\sigma_F = |F| \sqrt{\left(\frac{\sigma_C}{C}\right)^2 + \left(\frac{\sigma_B}{B}\right)^2}$$

Here, F is the relative change calculation at each vial, C is the difference operation (*C*=*A*-*B*) of the median value of reference vial from that of each vial, and B is the median value of the reference vial.

Specific Aims

Aim 1. Determine if T1ρ is more sensitive to pH changes than T2.

Two phantoms were created to help determine T1ρ sensitivity to changing pH. First, vials with coarse variation in pH values were imaged then a tighter physiologically relevant pH range within the coarse range was imaged. If these large and small changes are distinguished in quantitative T1ρ then credence is given to T1ρ sensing local pH variation *in vivo*. The dependence of T1ρ pH sensitivity on temperature was included in this study. Knowing that temperature affects proton transfer rates, the effects of changing temperature might be reflected in the relaxation parameters. This could then inform about the mechanisms each parameter is observing. Temperature in vials were brought approximately to 0, 22 and 36 °C to be imaged. Among the three experiments described below, two were conducted at 22 °C and the third at 0 and 36 °C. Quantitative T1ρ, T2 and T1 values were collected.

It was hypothesized in these experiments that:

1. T1ρ values would increase as pH decreases.
2. T1ρ will be more sensitive to pH than T2.
3. T1ρ will remain linear in trend at 0, 22 and 36 °C temperatures.
4. T1ρ will be more responsive than T2 at all of the temperatures.

Experiment 1.1:

A phantom with 7 vials was created. All vials were filled to 45ml with liquid egg-white. Added to 3 of the 7 vials were 0.5, 1.0 and 1.5mL HCl. The resulting pH values were 9.02 (no HCl nor H_2O), 8.24, 7.21 and 6.74 respectively. The other 3 had 0.5, 1 and 1.5ml of deionized water added. Respective pH values of vials with added water are 9.03, 9.04 and 9.05. An *Accumet AB15* pH meter was used to collect the pH values reported. The vials with water were to act as a control for water content contribution to T1ρ. Presented in Table 2.1 are the sequence parameters used to measure the relaxation times for T1ρ, T2 and T1. The container (Figure 2.5) for the vials was filled with room temperature in this experiment, the vials were imaged at approximately 22 °C.

Table 2.1: Scan parameters for Experiment 1 of Aim 1

	T1ρ	**T2**	**T1**
TSL (ms)	0, 20, 40, 60, 80, 100	N/A	N/A
Spin-Lock Freq. (Hz)	400	N/A	N/A
Preparation TE (ms)	N/A	0, 20, 40, 60, 80, 100	N/A
TI (ms)	N/A	N/A	50, 300, 500, 900, 1500, 2300
TR (ms)	5000	5000	10,000
FOV (cm^2)	12.8×12.8	12.8×12.8	12.8×12.8

BW (Hz/px)	130	130	130
Matrix	512×256	512×256	256×64
Flip Angle	180°	180°	180°
Slice thickness (mm)	5.0	5.0	5.0
Turbo Factor	4	4	N/A
Echo spacing (ms)	12.2	12.2	N/A
Sequence TE (ms)	14	14	12

Experiment 1.2:

A second phantom with 7 vials was created. Each vial was filled with 45ml of a 315ml batch solution of liquid egg-white. The batch solution was stirred as HCl was being added. The pH value of the solution was monitored and was poured out as the pH value read 7.5, 7.3, 7.18, 6.96, 6.76, 6.6, and 6.51. Table 2 below has the spin-lock, echo, inversion times and TSE parameters for this experiment. The setup before imaging was identical in temperature and container to that of Experiment 1.1.

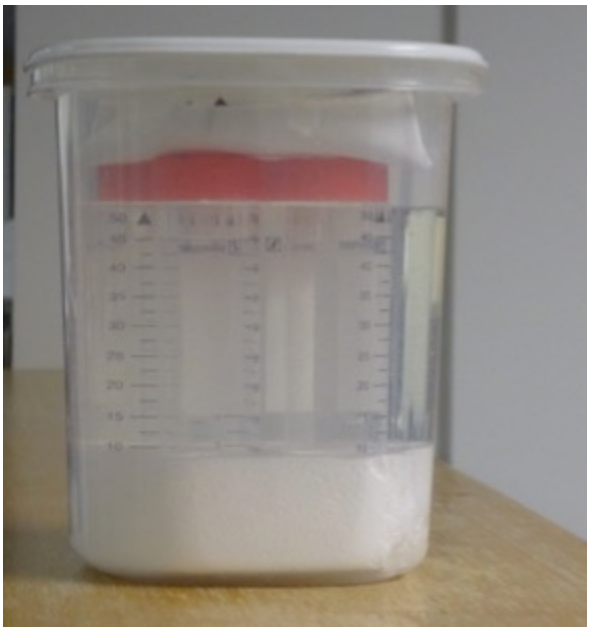

Figure 2.5: Container used for Experiment 1.1 of Aim 1.

Table 2.2: Scan parameters for Experiment 2 of Aim 1.

	T1ρ	T2	T1
TSL (ms)	0, 100	N/A	N/A
Spin-Lock Freq. (Hz)	400	N/A	N/A
Preparation TE (ms)	N/A	0, 100	N/A
TI (ms)	N/A	N/A	50, 150, 250, 450, 750, 1150
TR (ms)	5000	5000	5000
FOV (cm^2)	12.8×12.8	12.8×12.8	12.8×12.8
BW (Hz/px)	130	130	130
Matrix	256×256	256×256	256×256
Flip Angle	180°	180°	180°
Slice thickness (mm)	5.0	5.0	5.0
Turbo Factor	4	4	10
Echo spacing (ms)	12.2	12.2	9.51
Sequence TE (ms)	13	13	9.5

Experiment 1.3:

The dependence of T1ρ and T2 sensitivity to pH on temperature was explored in this experiment. In addition to imaging the relaxation times at 22 °C in Experiments 1.1 and 1.2, the phantom from Experiment 1.2 was also imaged at approximately 0 and 36 °C. For 0 °C experiment, crushed ice was packed lightly into the container holding with a small amount of water. The 36 °C experiment was performed by pouring water heated from the microwave into the container. Temperature of the egg-white was monitored using a temperature sensor (*ReFlex*; Neoptix, Inc., Québec, Canada) with fiber optic probes before and after scanning. A piece of Styrofoam was fashioned to fit into the top of the container and an opening was made where the temperature probe could be inserted. To slow the drift of temperature during scans, the interior of the head coil and exposed portions of the container were padded with towels. These experiments might give insight into how T1ρ and T2 sensitivity changes as temperature is varied.

Quantitative T1ρ and T2 were measured in these experiments and temperature values were recorded before and after each imaging session.

Table 2.3: Scan parameters Experiment 3 of Aim 1

	T1ρ	**T2**
TSL (ms)	0,100	N/A
Spin-Lock Freq. (Hz)	400	N/A
Preparation TE (ms)	N/A	0, 100
TR (ms)	5000	5000
FOV (cm^2)	12.8×12.8	12.8×12.8
BW (Hz/px)	130	130
Matrix	256×256	256×256
Sequence TE (ms)	13	13
Flip Angle	180°	180°
Slice thickness (mm)	5.0	5.0
Turbo Factor	4	4
Echo spacing (ms)	12.2	12.2

Aim 2. Determine if T1ρ is more sensitive to glucose changes than T2.

T1ρ sensitivity to glucose changes was determined by imaging three phantoms. The phantoms differed in range of concentration. This was done to check which range would evoke the greatest change in T1ρ at 3T. The degree of change in T1ρ values at either range may clarify which is the greatest contributor to T1ρ signal in the brain, pH or glucose. Temperature was also varied in one of the phantoms to determine the dependence of glucose sensitivity on temperature. Varying temperature at which quantitative relaxation measurements are taken could inform about mechanisms being

imaged since the relaxation parameters might behave differently. Quantitative T1ρ, T2 and T1 values were retrieved from the scanning sessions at 22 °C but only T1ρ and T2 for 0 and 36 °C. Three experiments were conducted to determine sensitivity to glucose concentration changes and are described below.

Hypotheses for these experiments include:

1. T1ρ will decrease with increasing glucose conc.
2. T1ρ will be more sensitive than T2 to glucose changes
3. T1ρ will remain linear in trend at 36, 0 and 22 °C
4. T1ρ will be more responsive than T2 at all of the temperatures

Experiment 2.1

A phantom of 4 vials was created. Each vial was filled with 45ml of 325ml batch solution of a standard pH 7 phosphate buffer saline (PBS; BDH, VWR Analytical; Radnor, PA). Before filling the vials with the solution, 0.1mM Mn(II)Cl was added while stirring the solution. The metal in Mn(II)Cl served as a relaxation agent to decrease the observed relaxation times closer to that of brain tissue. Glucose concentrations of 0, 5, 10 and 20mM were then added to the 4 vials, which were placed into a polyethylene cylindrical container containing the water bath. Properties of the imaging session for this experiment are found in Table 2.4. This phantom was imaged at 22 °C

Table 2.4: Scan properties for Experiment 1 of Aim 2.

	T1ρ	**T2**	**T1**
TSL (ms)	0, 20, 40, 60, 80, 100	N/A	N/A
Spin-Lock Freq. (Hz)	400	N/A	N/A
Preparation TE (ms)	N/A	20, 40, 60, 80, 100	N/A

TI (ms)	N/A	N/A	50, 150, 250, 450, 750, 1150
TR (ms)	5000	5000	10,000
FOV (cm^2)	12.8×12.8	12.8×12.8	12.8×12.8
BW (Hz/px)	130	130	130
Matrix	512×256	512×256	256×64
Flip Angle	180°	180°	180°
Slice thickness (mm)	5.0	5.0	5.0
Turbo Factor	4	4	N/A
Echo spacing (ms)	12.2	12.2	N/A
Sequence TE	14	14	13

Experiment 2.2:

The setup of Experiment 2.1 was then repeated with a broader range of concentrations. Glucose concentrations were 0, 20, 50 and 100mM. Concentrations were increased to explore a broader range since the smaller concentrations may not be detectable at 3T. With a larger range, the increase in exchangeable protons might be noticeable at 3T. Properties of the imaging session for this experiment are found in Table 2.5. This experiment was conducted at 22 °C

Table 2.5: Scan properties for Experiment 2 of Aim 2.

	T1ρ	**T2**	**T1**
TSL (ms)	0, 20, 40, 60, 80, 100	N/A	N/A
Spin-Lock Freq. (Hz)	400	N/A	N/A
Preparation TE (ms)	N/A	0, 20, 40, 60, 80, 100	N/A
TI (ms)	N/A	N/A	50, 150, 250, 450, 750, 1150
TR (ms)	5000	5000	10,000
FOV (cm^2)	12.8×12.8	12.8×12.8	12.8×12.8

BW (Hz/px)	130	130	130
Matrix	512×256	512×256	256×64
Flip Angle	180°	180°	180°
Slice thickness (mm)	5.0	5.0	5.0
Turbo Factor	4	4	N/A
Echo spacing (ms)	12.2	12.2	N/A
Sequence TE	14	14	12

Experiment 2.3:

A phantom of 5 vials was filled with a PBS solution of Mn(II)Cl as described in Experiment 2.1. Before filling the vials with the solution, the solution was titrated to a pH of 6.52 with HCl. The pH of the solution was changed to see if increased acidity would change the relaxation rates when compared to the Experiment 2.1 at 22 °C Glucose concentrations 0, 15, 30, 45 and 60mM were then added to the 5 vials. These vials were then imaged at 0, 22, and 36 °C.

The plastic container in Figure 2.5 was used for the three imaging experiments. The setup for 0 and 36 °C before imaging was identical to that of Experiment 1.3. The temperature of the water in the container was monitored, not the liquid in the vials. These experiments might give insight into T1ρ's response to glucose changes at different temperatures. Properties of the imaging session for this experiment are found in Table 2.6. Quantitative T1ρ and T2 were measured in these experiments. Temperature values were recorded before and after each the imaging session.

Table 2.6: Scan properties for Experiment 3 of Aim 2.

	T1ρ	**T2**
TSL (ms)	0,100	N/A
Spin-Lock Freq. (Hz)	400	N/A

Preparation TE (ms)	N/A	0, 100
TR (ms)	3000	5000
FOV (cm^2)	12.8×12.8	12.8×12.8
BW (Hz/px)	130	130
Matrix	256×256	256×256
Flip Angle	180°	180°
Slice thickness (mm)	5.0	5.0
Turbo Factor	4	4
Echo spacing (ms)	12.2	12.2
Sequence TE (ms)	13	13

Aim 3: Determine if T1ρ is sensitive to lysine.

Sensitivity of T1ρ to variation in lysine concentration was determined by imaging one phantom. The two electrophilic NH_3^+ groups in the structure of lysine allow for amide proton transfer. Since amide proton transfer can be detected at 3T it might be possible to detect changes in lysine concentration. If these changes are noticeable, then it might give evidence for the contribution of charged structures to T1ρ variation in the brain. Temperature was also varied in the lysine phantoms to determine the dependence of lysine sensitivity on temperature. The reason for doing this is similar to the temperature experiments in the glucose experiment. Below are the hypotheses for the experiments conducted with lysine.

Hypotheses:

1. T1ρ will decrease with increasing lysine conc.
2. T1ρ will remain linear in trend at 36, 0 and 22 °C.
3. T1ρ will be more responsive than T2 at all of the temperatures

Experiment 3.1:

A phantom of 5 vials was created. Each vial was filled to 45ml with batch solutions of mono- and di- basic phosphate salts for consistent pH of 6.5. Included with

the salts solutions was a 20X solution of 0.1mM Mn(II)Cl. Lysine concentrations 0, 1.5, 3.0, 4.5 and 6.5mM were then added to all 5 vials. Properties of the imaging session for this experiment are found in Table 2.7.

Table 2.7: Scan parameters for Experiment 1 of Aim 3.

	T1ρ	T2	T1
TSL (ms)	0,100	N/A	N/A
Freq. (Hz)	400	N/A	N/A
Preparation TE (ms)	N/A	0, 100	N/A
TR (ms)	5000	5000	5000
FOV (cm^2)	12.8×12.8	12.8×12.8	12.8×12.8
BW (Hz/px)	130	130	130
Matrix	256×256	256×256	256×256
Flip Angle	180°	180°	180°
Slice thickness (mm)	5.0	5.0	5.0
Turbo Factor	4	4	10
Echo spacing (ms)	12.2	12.2	9.51
Sequence TE (ms)	13	13	9.5

Experiment 3.2

Dependence of temperature on lysine sensitivity of T1ρ was explored with the phantom. The phantom described in Experiment 3.1 was imaged and the set up for the 0 and 36 °C experiments of Experiment 1.3 was used in these experiments. Temperature values were recorded before and after each the imaging session.

Table 2.8: Scan parameters for Experiment 2 of Aim 3.

	T1ρ	T2
TSL (ms)	0,100	N/A
Freq. (Hz)	400	N/A

Preparation TE (ms)	N/A	0, 100
TR (ms)	5000	5000
FOV (cm^2)	12.8×12.8	12.8×12.8
BW (Hz/px)	130	130
Matrix	512×256	512×256
Flip Angle	180°	180°
Slice thickness (mm)	5.0	5.0
Turbo Factor	4	4
Echo spacing (ms)	12.2	12.2
Sequence TE (ms)	14	14

Aim 4: Observe relaxation in both pH and metabolite phantoms for a dispersion effects.

In the pH, glucose and lysine sensitivity experiments, dispersion studies were also conducted. Dispersion refers to the measurement of T1ρ at various spin-lock frequencies. For the pH phantom, which contains egg-white protein, changes in T1ρ at different frequencies might say something about the restrictions to the rotation water molecules bound to the proteins. The metabolite phantoms might speak about the amount proton exchange occurring between water molecules and metabolites. Quantitative T1ρ was performed at varying RF energy, which translated to varied frequencies. The hypothesis for this

Hypothesis:

T1ρ values will increase as the spin-lock frequency increases in imaging pH and glucose phantoms.

Experiment 4.1:

Phantoms described in Experiments 1.1 and 1.2 of Aim 1 were used in dispersion experiments. Scans for both phantoms shared the same properties as presented on Table 2.9.

Table 2.9: Scan parameters of dispersion experiments in pH phantoms

	T1ρ
TSL (ms)	0,100
Freq. (0.1kHz)	2, 4, 6, 8
TR (ms)	5000
FOV ($\mathbf{cm^2}$)	12.8×12.8
BW (Hz/px)	130
Matrix	512×256
Flip Angle	180°
Slice thickness (mm)	5.0
Sequence TE (ms)	14
Turbo Factor	4
Echo spacing (ms)	12.2

Experiment 4.2:

Glucose phantoms described in Experiment 2.1 of the glucose sensitivity study was also used in a dispersion experiment. The phantom described in was scanned with the properties shown in Table 2.10.

Table 2.10: Properties of dispersion experiment for glucose phantom

	T1ρ
TSL (ms)	0,100

Freq. (0.1kHz)	2, 4, 6, 8
Sequence TE (ms)	14
TR (ms)	5000
FOV (cm^2)	12.8×12.8
BW (Hz/px)	130
Matrix	512×256
Flip Angle	180°
Slice thickness (mm)	5.0
Turbo Factor	4
Echo spacing (ms)	12.2

Experiment 4.3:

A dispersion experiment was conducted for the lysine phantom experiment. Properties of the scan performed for this are presented in the Table 2.10

Table 2.11: Properties of dispersion Experiment 3.1 phantom.

	T1ρ
TSL (ms)	0,100
Freq. (0.1kHz)	2, 4, 6, 8
Sequence TE (ms)	14
TR (ms)	5000
FOV (cm^2)	12.8×12.8
BW (Hz/px)	130
Matrix	512×256
Flip Angle	180°
Slice thickness (mm)	5.0
Turbo Factor	4
Echo spacing (ms)	12.2

RESULTS

Aim 1

Experiment 1.2

In this experiment, seven vials were imaged. All seven contained liquid egg-white but the three with acid included had pH values as shown in Figure 1.1a. Vials with added water had pH resembling that of the center vial that contained only liquid egg-white. Water was added to the three vials as a control for contribution of water content to the pH dependence of T1ρ. Data for control vials are not presented but they were, the percent change in T1rho and T2 was between 0 and 4%, which is nominal compared to the response shown in Figure 3.1e. Figures 3.1b-d show the T1ρ, T2 and T1 maps for the coarse pH range phantom.

Of the hypotheses formed for Aim 1, those pertaining to this experiment include: (1) T1ρ values would increase as pH decreases, (2) T1ρ will be more sensitive to pH than T2 and (3) T1ρ will remain linear at 22 °C. As it is shown Figure 1.1e, T1ρ does increase with decreasing pH values. However T2 seems to show more sensitivity to pH changes in the 6.99 – 6.4 range, having a slope of 50.8 compared to 25.4 of T1ρ in that range. T2 also appears to be constant in the 6.99 – 8.4 range. T1, in the same range, seem to be responsive with a slope of approximately -8.6. This result shows that T1ρ has a large dynamic range in coarse scale pH values when compared with T2 and T1, which seem unable to detected change some ranges.

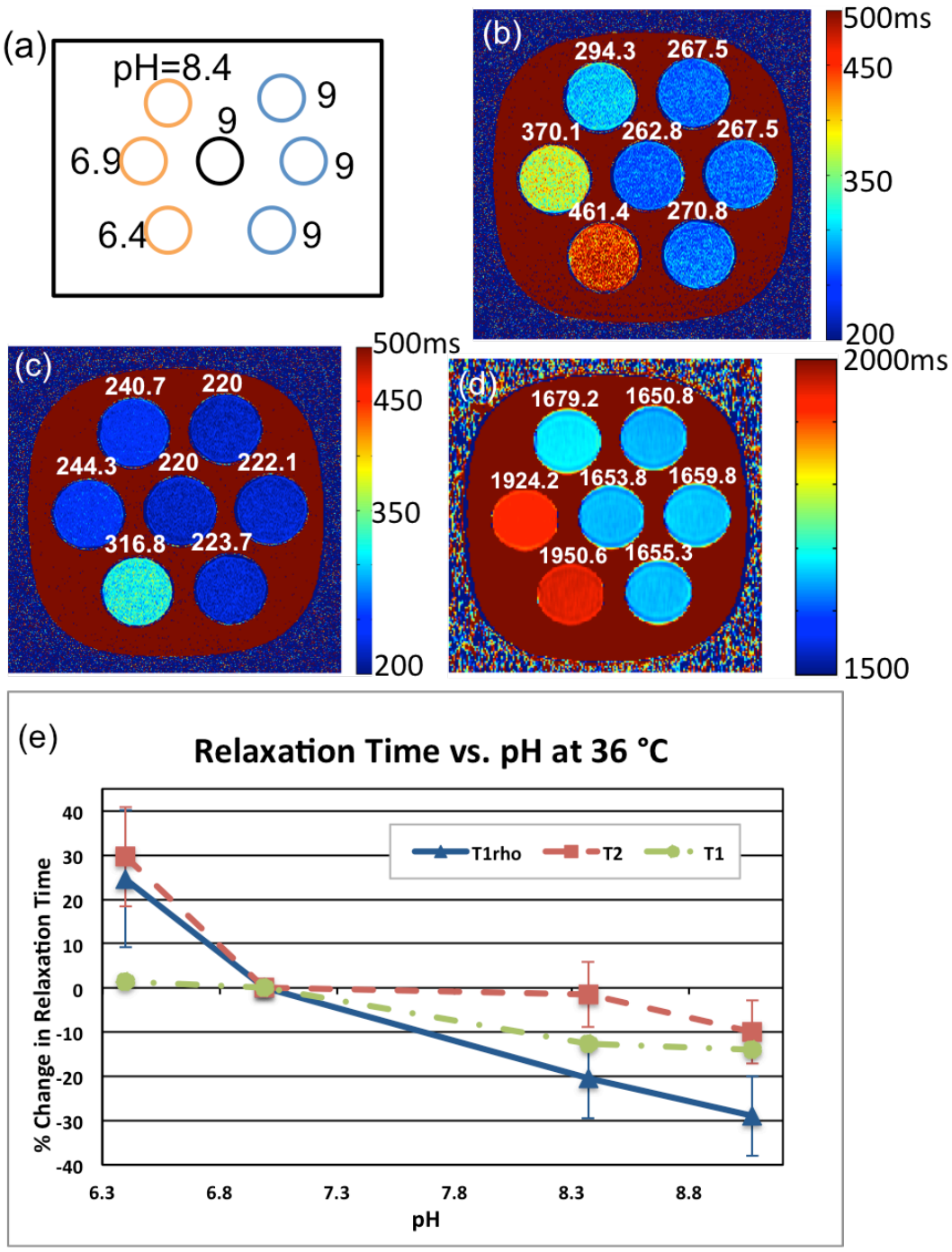

Figure 3.1: Shown here are the respective pH values of the vials (a) for Experiment 1.1 and its T1ρ (b), T2 (c) and T1 (d) maps. Above the vials in each map is the median relaxation time for each. Vials to the left of the center vial contain varying amounts of acid and those to the left have water included. Responses of the quantitative values are plotted with respect to the acidic vials in (e).

Experiment 1.2

Seven vials were imaged during this experiment. Each vial contained liquid egg-white and HCl to bring pH levels to the physiologically relevant range (7.5 – 6.5). Quantitative maps of T1ρ, T2 and T1 are displayed in Figure 3.2b, c and d respectively. The pH values corresponding to each vial can be found in Figure 3.2a and a plot in the median relaxation times from each map is plotted in Figure 3.2e. Looking at the maps, T1ρ seems to show the most response in the physiologic range because of the large variation in relaxation time across the vials. This is also reflected in the plot, where T1ρ is linear in the full range but for T2, there seems to be a plateau that corresponds with the plot in coarse range pH values. T1ρ and T2 are comparable in response in the 6.51 – 6.96 range. T1, however, was non responsive to the pH physiologically relevant range. This experiment was repeated twice and the same trend was seen.

Relating to the hypotheses formed for Aim 1, this experiment is in agreement that T1ρ increases as pH decreases. It also agrees that T1ρ is linear in trend at 22 °C. The sensitivity of T1ρ to changes in the physiologically relevant is also shown to be more than of T2 because of the minimal response seen in the pH range of 6.9 – 7.5.

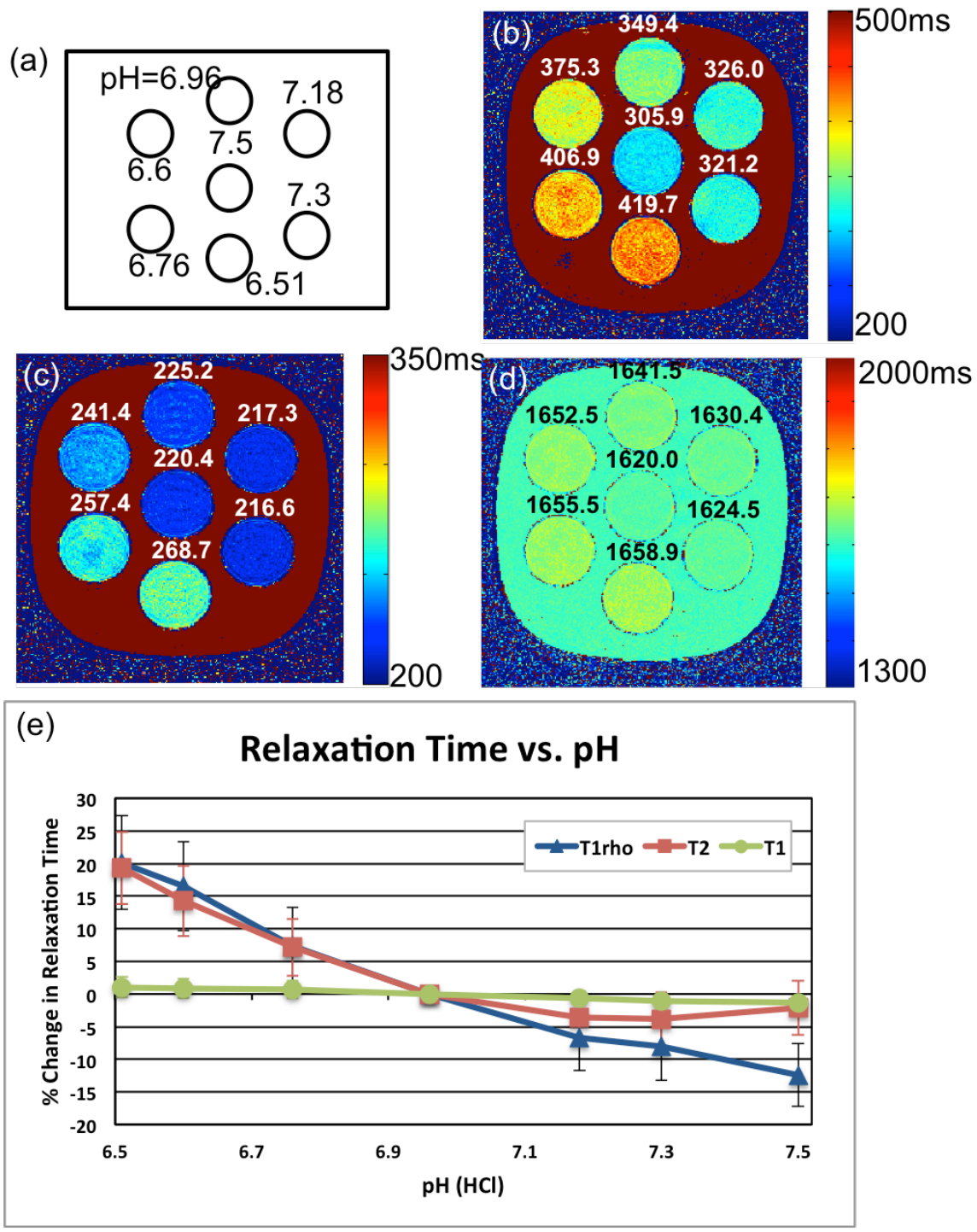

Figure 3.2: Results of the physiologically relevant pH range is shown here. Subfigure (a) is the respective pH values of each vial in the quantitative maps of T1ρ (b), T2 (c) and T1 (d). The median relaxation time for vial is recorded in each subfigure. All vials have acid added and the plot in (e) shows the percent change of each quantitative measure taken for this Experiment 1.2.

Experiment 1.3

The same set of vials used in Experiment 1.2 was used in this experiment. Figure 3.3 shows the results of the 0 °C experiment and Figure 3.4 shows the 36 °C experiment. In these experiments, only T2 and T1ρ were collected. Temperatures recorded before and after the 0 and 36 °C experiments were 0.3 – 0.1 °C and 37.2 – 34.8 °C respectively. Comparing the relaxation times recorded on the T1ρ maps for 0 and 22 °C, it can be said that the T1ρ values decreased at the colder temperature since the values at 22 °C ranged from 305.9–419.7 and that at 0 °C ranged from 274.1–358.2. Performing the same comparison with values recorded on the T2 maps shows that at 0 °C, T2 values did not change much in magnitude relative to the 22 °C. The effect of the cold temperature, however, is shown in Figure 3.3c where both T1ρ and T2 are linear in the full range. The plateau seen in the T2 at 22 °C is no longer present at 0 °C. These result could mean that the exchange of molecules may have decreased in frequency due to the effect temperature can have on exchange kinetics. Thus, the T1ρ response could be contributed to more by T2 than chemical exchange.

At 36 °C, the response T1ρ was nonlinear rather than linear as was seen at other temperatures (Figure 3.4c). Response of T2 seems to explain this result; because T2 relaxation contributes to T1ρ, it can be said that the usual linear trend is being affected by T2 where response starts to go negative. In the region where T1ρ is decreasing, T2 appears to be linear. Where T1ρ may have had a decreasing trend (after pH 6.96), T2 negates that decrease since its values are increasing in value after pH 6.96. This experiment was conducted three times and the plots of those trials are shown in Figure 3.5.

According to this experiment, the hypothesis stating that T1ρ will remain linear in trend at the three temperatures was wrong. T1ρ was not linear at 36 °C. T1ρ was not more responsive than T2 at all temperatures. However, T1ρ still increases with decreasing pH values.

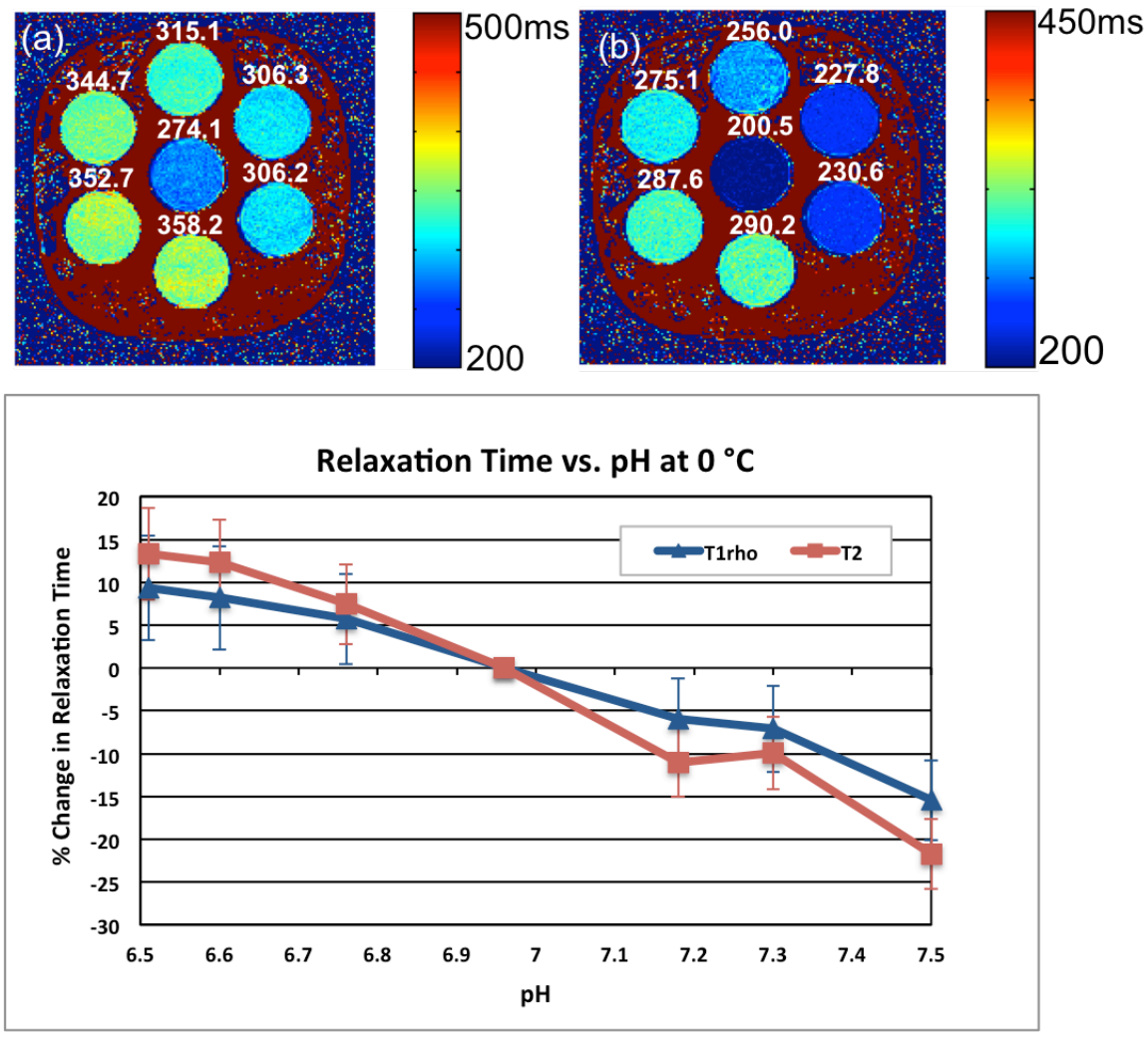

Figure 3.3: Results of the 0 °C experiment are displayed. The corresponding pH values are the same as in Figure 3.2a. Quantitative maps T1ρ (a) and T2 (b) were generated from the imaging session. The plot shown is the relative change in median relaxation time values with respect to the 6.96 vial.

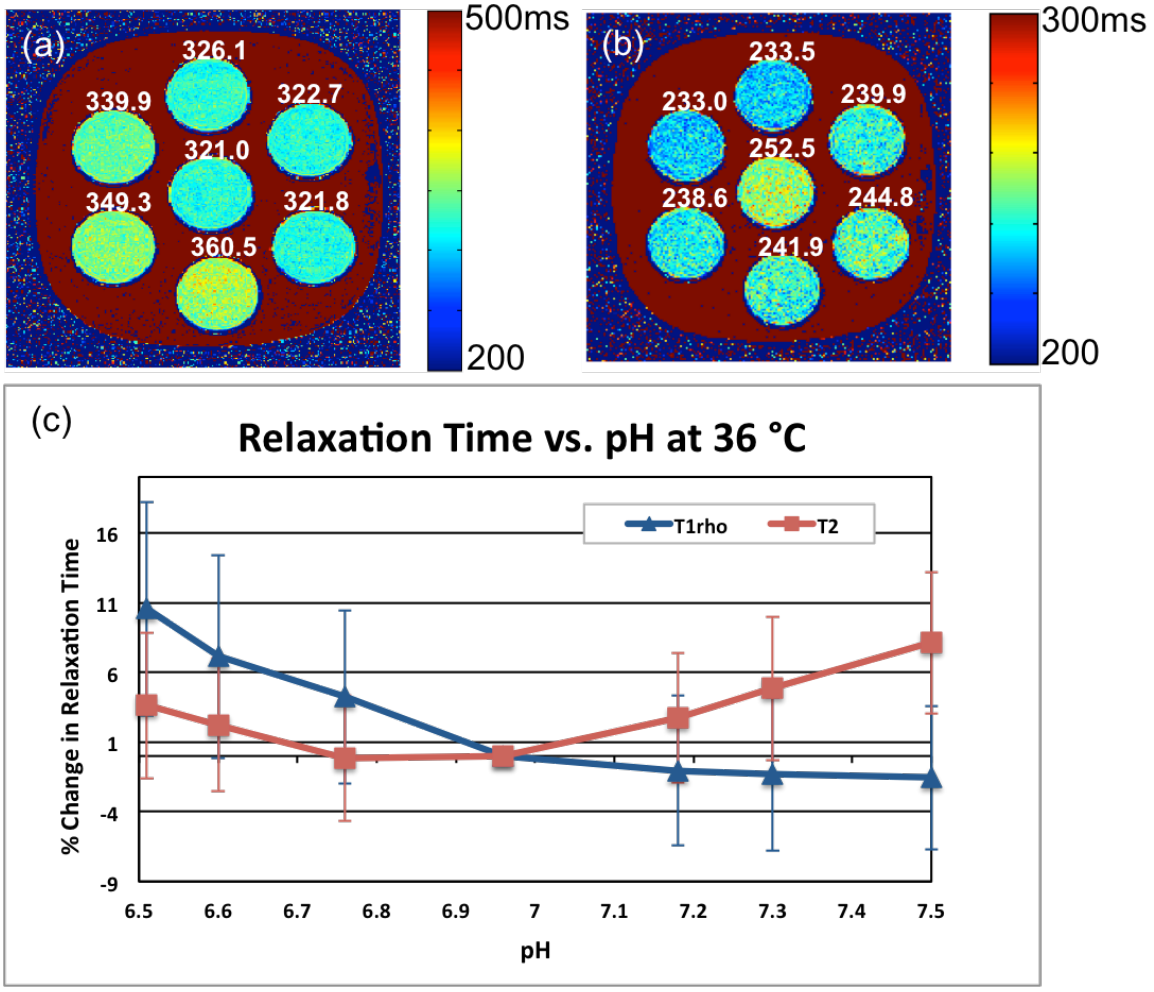

Figure 3.4: Results of the 36 °C experiment are shown here. The corresponding pH values are the same as in Figure 3.2a. Quantitative maps T1ρ (a) and T2 (b) were generated from the imaging session. The plot shown is the relative change in median relaxation time values with respect to the 6.96 vial.

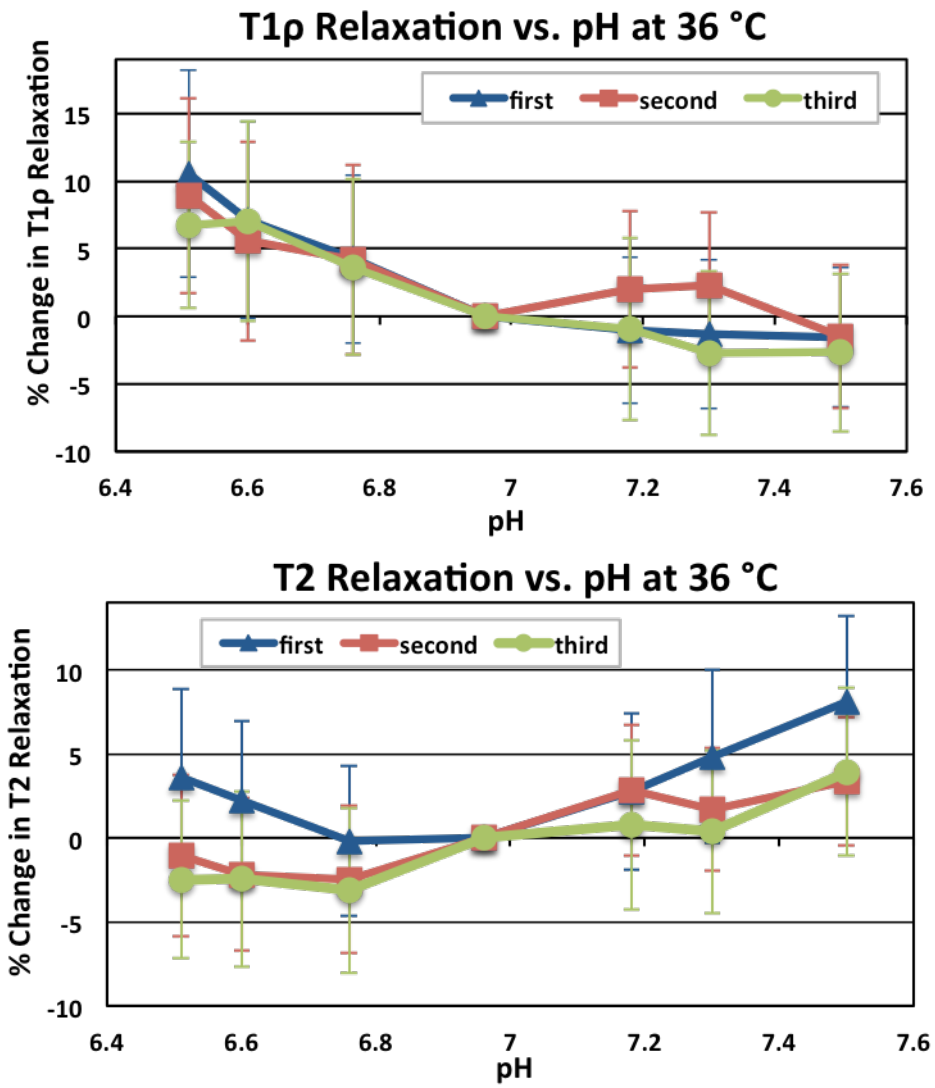

Figure 3.5: Pictured here are plots of relative change in T1ρ and T2 relaxation at 36 °C. This shows that the nonlinear trend is reproducible as this temperature experiment was performed three times.

Aim 2

Experiment 2.1

There were four vials imaged in this experiment. These vials contained varying concentrations of glucose within a phosphate buffered solution. Quantitative maps of T1ρ, T2 and T1 were generated and are present in Figure 3.6b-d respectively.

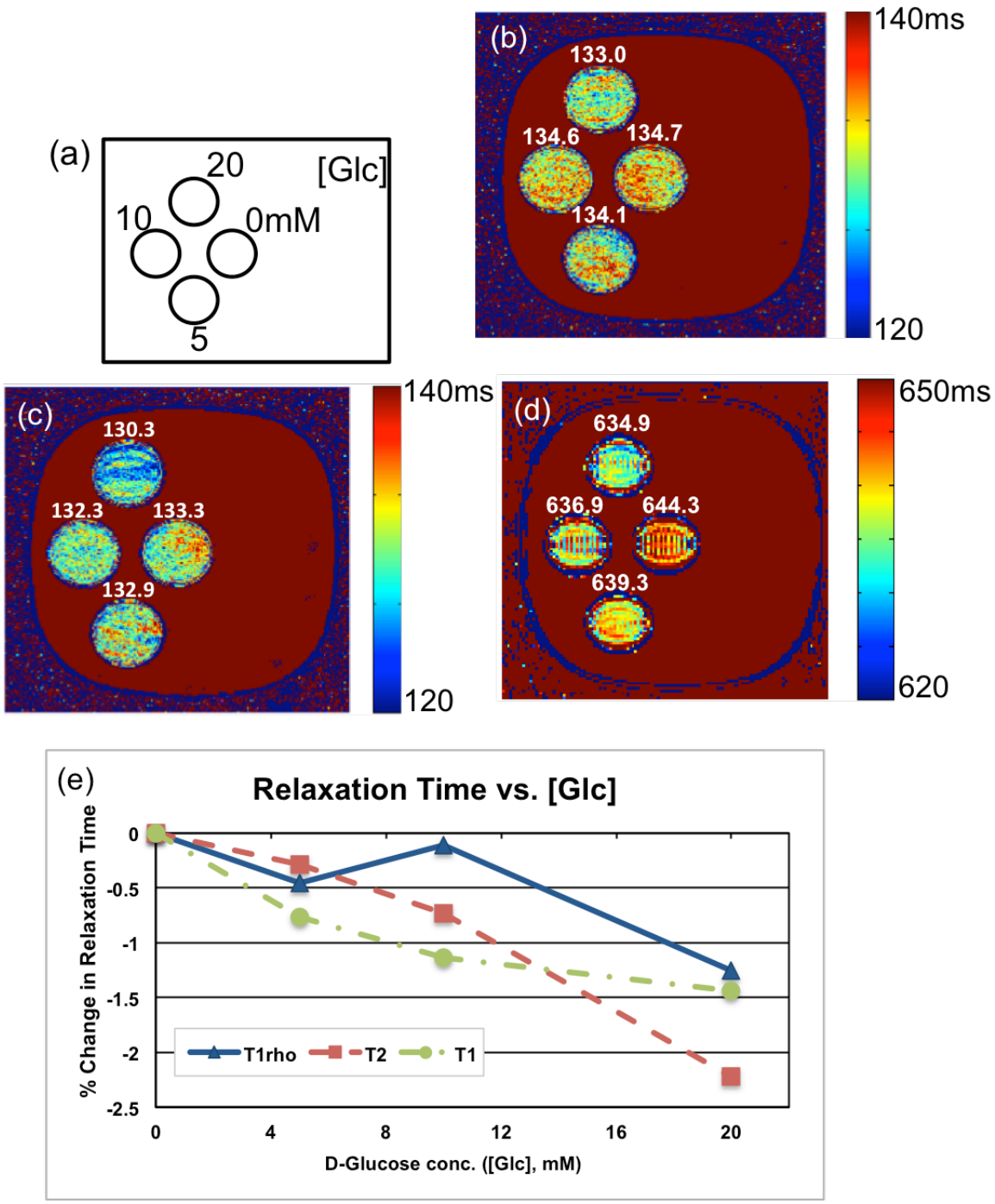

Figure 3.6: Results of Experiment 2.1 are shown here. The quantitative maps of T1ρ, T2 and T1 are shown in subfigures b, c and d. Diagramed in subfigure a are the respective glucose concentrations in the vials displayed in the maps. The plot shown in (e) is the relative change of the median relaxation times found in each vial.

Looking at these maps, it is clear that the relaxation times are much faster than those found in Aim 1. Even more apparent is the small amount of change observed for the range of glucose concentrations by the quantitative measures. It can be said that T1ρ is not sensitive to changes in glucose concentration in the range of 0 to 20mM at 3T. The response of T1ρ is least of the three relaxation parameters. Thus, relating to the hypotheses pertinent to this experiment, though there is a downward trend in T1ρ, the degree of change displayed begs the question of whether noise or artifact may be source of the change seen. Also, the same can be said of response of T2; though the response is higher than T1ρ, the degree of change is too small to be certain of the trend being observed.

Experiment 2.2

A larger range of glucose concentrations were imaged to see if a larger response could be evoked from the relaxation parameters. The concentrations are presented below in Figure 3.7a. By adding increasing the concentration within the vials, it can be said that the relaxation times decreased when compared with the maps of the previous experiment. According to the corresponding plots, the response was increased but the similarity of the three parameters means something else is driving the change being observed. Viscosity of the glucose solution is probably what is causing the observed change. The reason for this is because viscosity is known to increase linearly with glucose concentrations and that linearity is being reflected in the relaxation times. This then shows that in a wider range of glucose concentrations, T1ρ is more responsive to the viscosity of the solution at 3T.

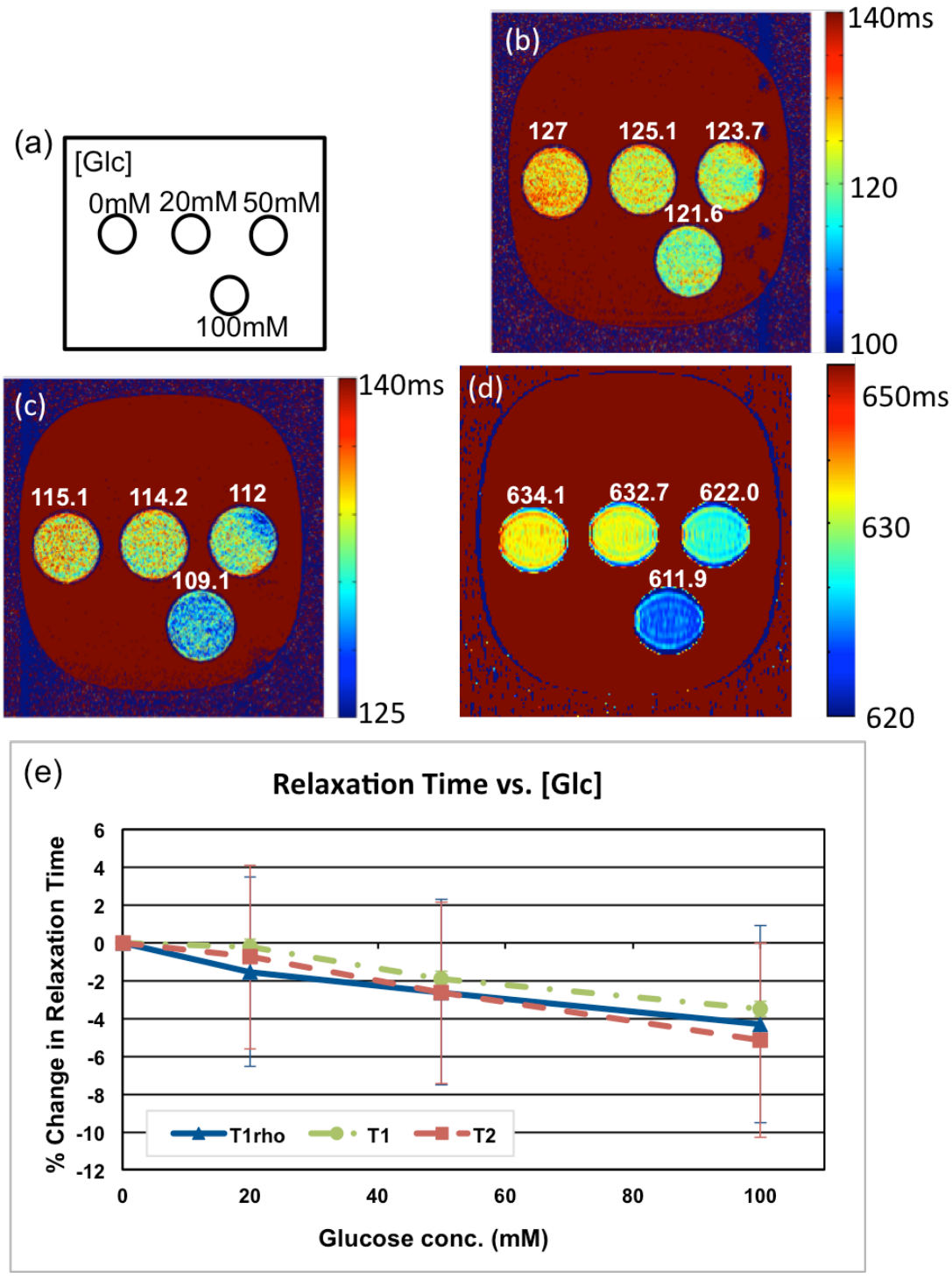

Figure 3.7: Results of Experiment 2.2 are shown here. The quantitative maps for T1ρ, T2 and T1 are presented and the glucose concentration of each vial is given by diagram. The plots of median relaxation time with respect to each vial is also shown.

Experiment 2.3

An intermediate range of glucose concentrations was used for the 0 and 36 °C experiments. These experiments were also conducted at a lower pH value than Experiments 2.1 and 2.2, these were at pH 6.5 instead of 7.5. The T1ρ and T2 maps are presented in Figure 3.8a, b for 0 °C and Figure 3.9a, b for 36 °C. Temperatures recorded before and after the 0 and 36 C experiments were 0.5 - 1.5 °C and 37.7 – 34.5 °C respectively. In the intermediate concentration range, the relaxation times are longer than what was observed in previous experiments. The reason might be because of the difference in the pH of the solutions.

From the plots of relative change, it can be said that T1ρ and T2 are responding similarly to the changes glucose concentration at either temperature. The results of these experiments are not in agreement with the hypothesis stating that T1ρ will be more responsive than T2 at all temperatures. Both T1ρ and T2 are similar in response so T1ρ is not more responsive than T2. T1ρ was linear in trend at 0, 36 °C and 22 °C, however, the cause of the linearity may not be due to hydroxyl proton exchange.

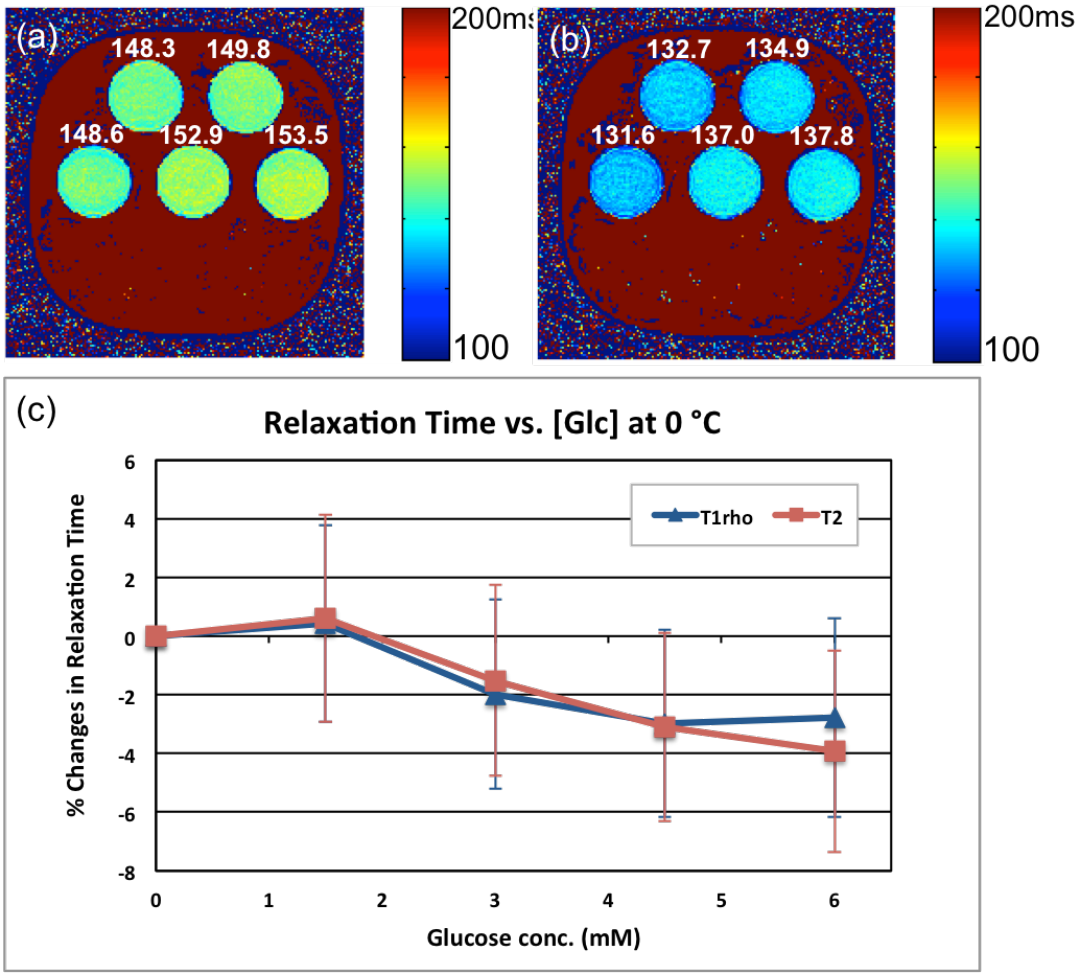

Figure 3.8: Results of the 0 °C experiment with the intermediate range glucose phantom. The concentrations of glucose in the vials are as follows, the center 0mM but starting from the right of the center vial and counterclockwise, those vials have 15, 30, 45 and 60mM. The subfigures a and b are the T1ρ and T2 maps respectively. Plots of subfigure c are the median relative relaxation time changes for each vial.

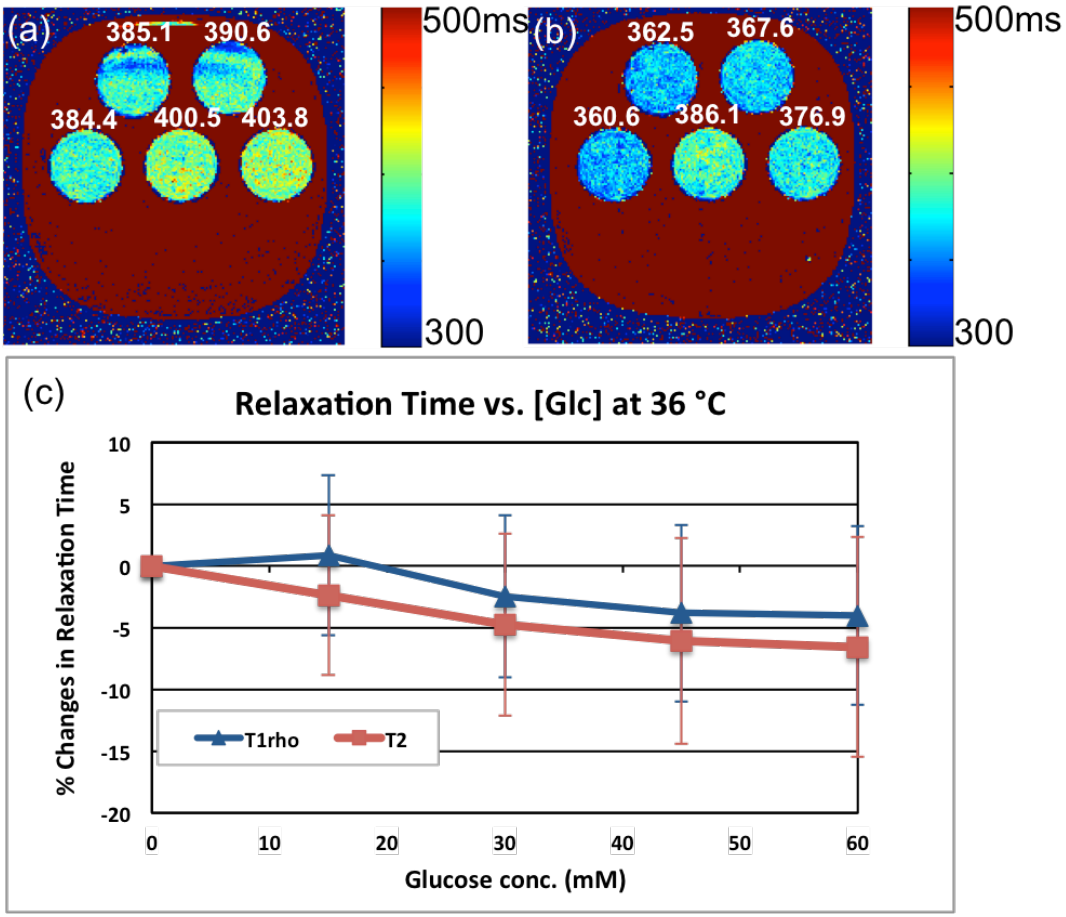

Figure 3.9: Results of the 36 °C experiment with the intermediate range glucose phantom. The concentrations of glucose in the vials are as follows, the center 0mM but starting from the right of the center vial and counterclockwise, those vials have 15, 30, 45 and 60mM. The subfigures a and b are the T1ρ and T2 maps respectively. Plots of subfigure c are the relative relaxation time changes using the median value relaxation value of each vial.

Aim 3

Experiment 3.1

Five vials containing varying concentrations of lysine HCl were imaged in this experiment. The goal of this experiment was to determine T1ρ sensitivity to changes in lysine concentrations. The concentrations used were kept low to match lysine concentrations in the body. The quantitative maps generated for this experiment are shown in Figure 3.10b (T1ρ) and c (T2). The relaxation time recorded these maps show

quicker relaxation times, faster than glucose, which had values between 100 and 130ms for both maps. Looking at the corresponding plot in Figure 3.10d, it can be said that the relaxation times are not sensitive to lysine concentration changes at 3T. The effect of charge to exchange rates cannot be evaluated because of the small change seen in T1ρ and T2.

Of the hypotheses made for Aim 3, those pertaining to this experiment include: (1) T1ρ will decrease with increasing lysine concentration and (2) T1ρ will remain linear in trend at 22 °C. This experiment does not answer the question because the response is low of both quantitative measure is low and the error in the measurement may be driving the changes seen. At 22 °C, T1ρ is not more responsive than T2.

Experiment 3.2

The vials imaged in Experiment 3.1 were also imaged for this experiment. Quantitative maps for the 0 and 36 °C experiments are displayed in Figure 3.11a, b and 3.12a, b. Temperatures recorded before and after the 0 and 36 °C experiments were 0.6 - 1.1 °C and 37.7 – 34.1 °C respectively. Comparing relaxation values at 0 and 36 °C to 22 °C, it is clear that the cold temperature decreased the relaxation times while the hot increased the relaxation times. The plots still show that T1ρ is similar in response to T2 at both temperatures.

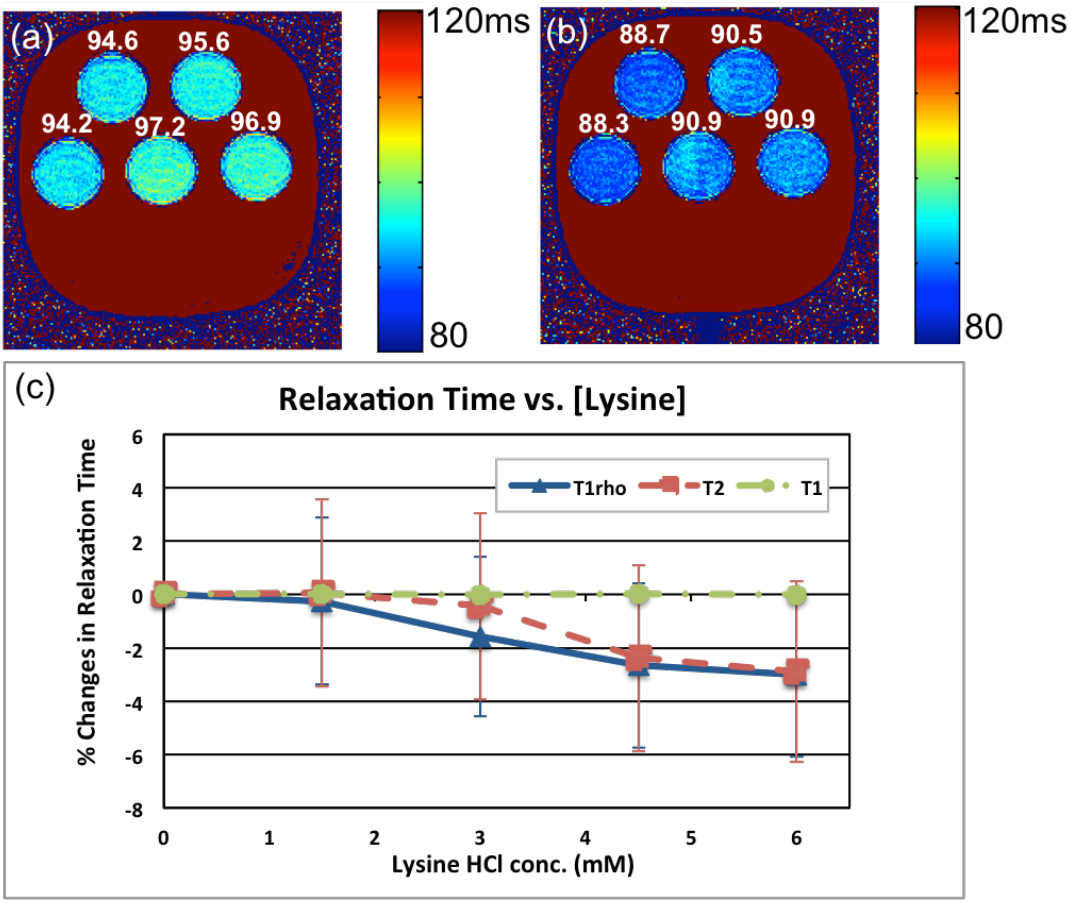

Figure 3.10: Provided in this figure are the quantitative maps of T1ρ and T2. Subfigure b is theT1ρ map and subfigure c is the T2 map. The plot in (d) is the relative relaxation time changes with respect to the lysine concentration. Lysine concentration for the center vial is 0mM; starting from the right of the center vial and moving counterclockwise, the remaining vials contain: 1.5, 3.0, 4.5 and 6.0mM of lysine.

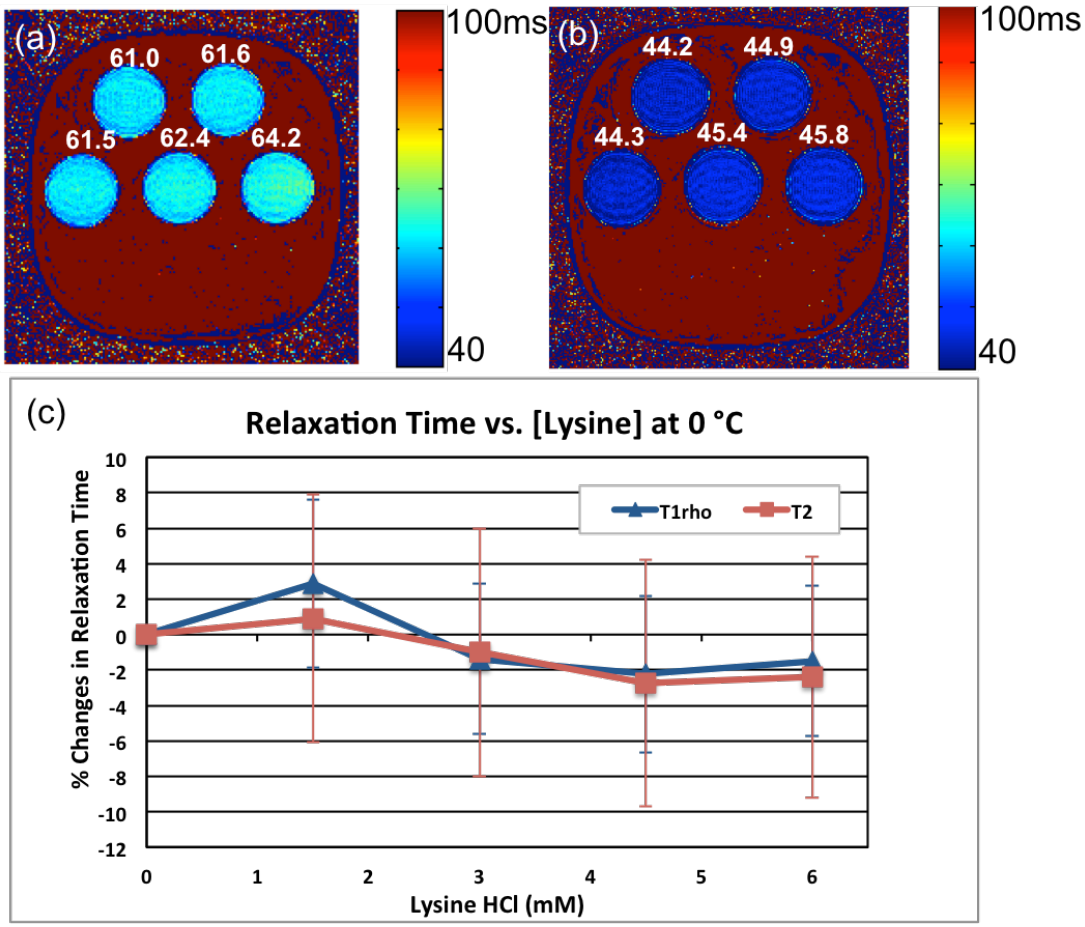

Figure 3.11: Results for the 0 C lysine experiment are displayed here. Subfigure a is theT1ρ map and subfigure b is the T2 map. The plot in (c) is the relative relaxation time changes with respect to the lysine concentration. The concentrations in each vial are the same as in Experiment 3.1

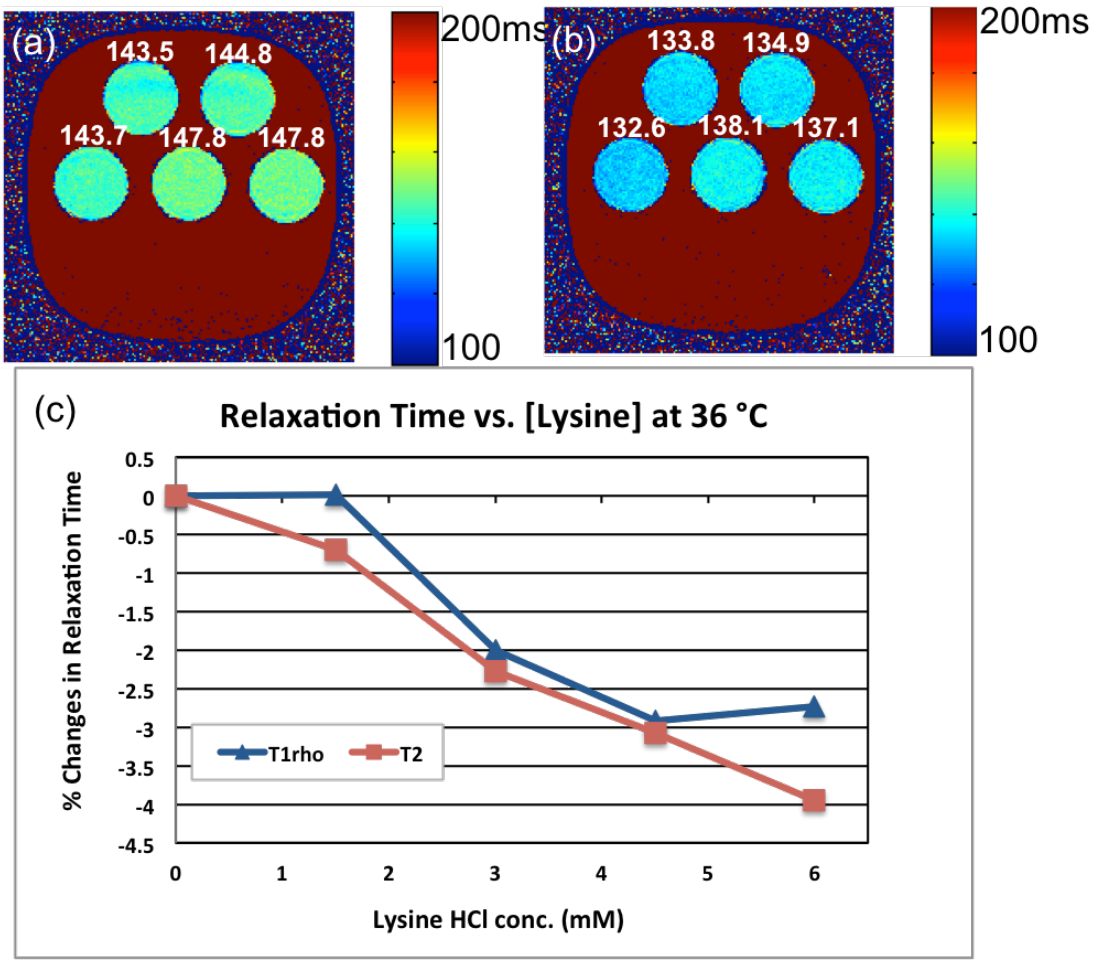

Figure 3.12: Results for the 36 C lysine experiment are displayed here. Subfigure a is the T1ρ map and subfigure b is the T2 map. The plot in (c) is the relative relaxation time changes with respect to the lysine concentration. The concentrations in each vial are the same as in Experiment 3.1.

Aim 4

Experiment 4.1

A dispersion experiment was conducted on the coarse scale pH phantom. The images for this experiment are not shown but the relative change plots are shown for each frequency. As can be seen, there is a frequency dependence on the exchanging molecules in this phantom. This is strongly suggested in the pH range of 7.18 to 9.0. Looking at the 200Hz response, it can be said that it resembles the T2 response shown in Figure 3.1. This suggests that there is more T2 contribution to the signal at that

frequency. The other frequencies get more linear in response as the spin-lock frequency is increased. There does not seem to be much frequency dependence in relaxation rates of exchanging molecules in the range of pH 6.6 to 7.1.

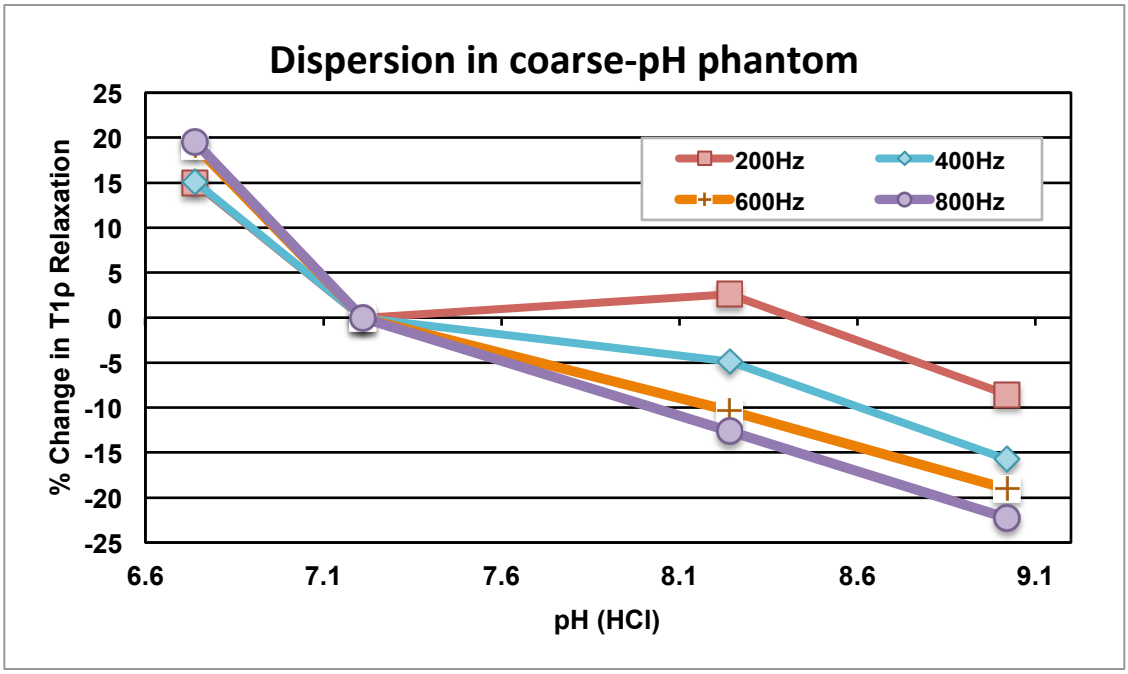

Figure 3.13: Dispersion result for coarse scale pH phantom of Experiment 1.1. The frequencies this phantom was imaged at were 200, 400, 600 and 800 Hz.

This experiment was conducted on the phantom with the physiologically relevant pH scale. The results of this experiment are displayed in Figure 3.14. On the pH range 6.5 – 7.3, there is no frequency dependence in the relaxation rates. However, in the 7.3 – 7.4 range, there is some dependence. The line shape of the 200Hz response resembles that of T2 shown in Figure 3.2, characteristic of the plateau in the 6.9 to 7.5 pH range.

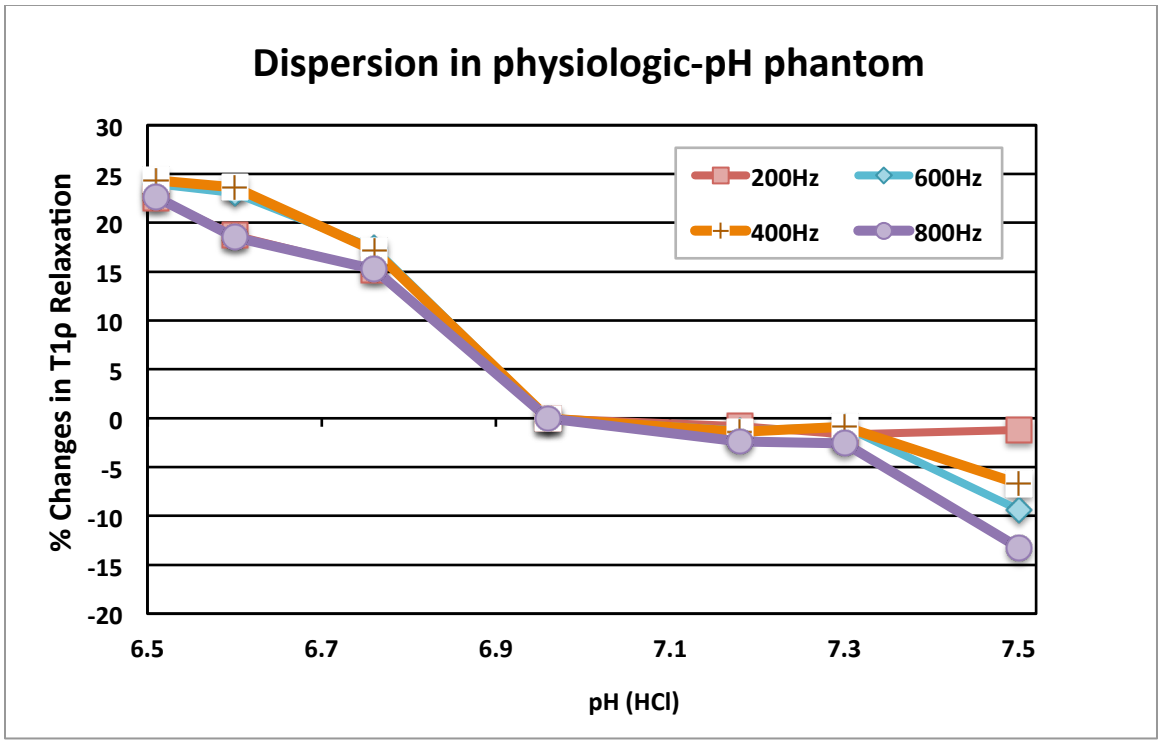

Figure 3.14: Results of the dispersion experiment conducted on the physiologically relevantly scaled pH phantom. The spin-lock frequencies used were 200, 400, 600 and 800Hz.

Experiment 4.2

The frequency dependence of the proton relaxation rates during hydroxyl exchange was measured by performing a dispersion experiment on the smaller scale of glucose concentrations. Figure 3.15 shows the results and it can be seen that there is some frequency dependence but because the response is low, it is difficult to interpret the results of this experiment.

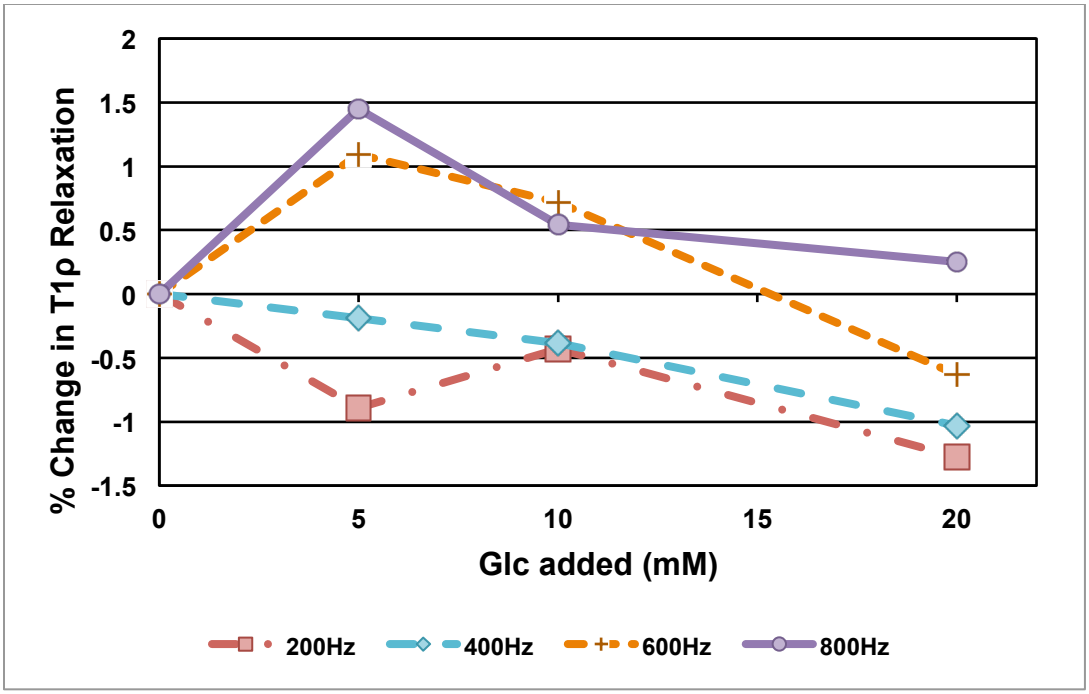

Figure 3.15: Results of the dispersion experiment on the phantom created for Experiment 2.1.

Experiment 4.3

The lysine phantom created for the Experiment 3.1 was used in this dispersion experiment. Results are displayed in figure 3.16 where it is clear that there is both low response and no frequency dependence on the relaxation rates of the interacting molecules in the phantom.

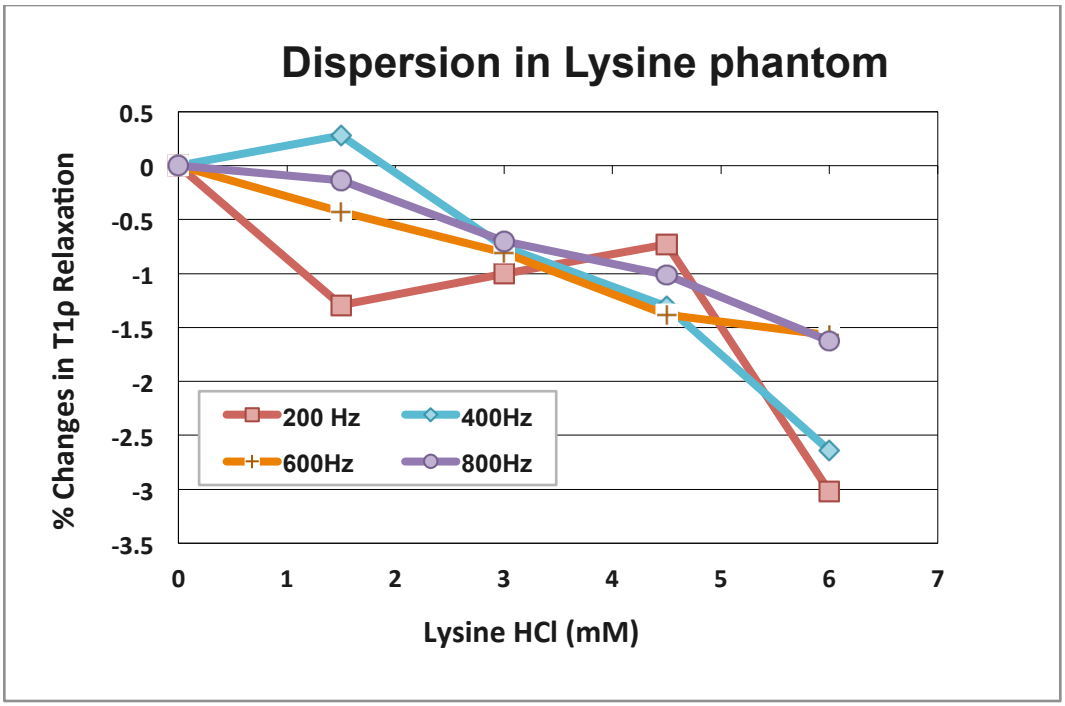

Figure 3.16: Results of the dispersion experiment on the phantom created for Experiment 3.1.

DISCUSSION

In this work, the temperature dependence of T1ρ sensitivity to metabolites such as pH, glucose and lysine was assessed. There were four aims devised in the for the experimentation and they are addressed in the following:

Aim 1: Determine if T1ρ is more sensitive to pH changes than T2

It was found that at body temperature, using a 3T scanner, T1ρ responds nonlinearly to the full range of the physiologic pH values (6.5–7.5). The nonlinear behavior is explained by the contribution of T2 relaxation to the response of T1ρ. This signifies the utility of measuring both T1ρ and T2 in an exchange system as it has been used by other researchers in quantifying the contribution of water content to T1ρ of tissue. Duvvuri *et al.* showed that water content was not a significant contributor to T1ρ changes when imaging cancer in mice because T2 did not vary much after the administration of a chemotherapy drug[25]. T2 variations were found to be small in vials with additional water content, also showing that water was not a contributing factor to T1ρ changes in these pH experiments. T1ρ was found to be sensitive to both finely and largely varying pH changes. This speaks of the advantage T1ρ has in detecting local variations in tissue acidity. The results at body temperature also show that T1ρ there is approximately a 10% drop in T1ρ for a 1 pH unit increase where as Kettunen *et al*. reported a 4.5% increase in a 1 pH unit drop in rat brain parenchyma. The difference in T1ρ response may be due to the difference in field strength at which both experiments were conducted; Kettunen's was at 4.7T but the difference in molecular composition may also be the reason for the difference in response of T1ρ to pH changes. Though the proteins are not the only constituents in tissue, these pH results show that at 3T, amide proton exchange is causing the greatest change in T1ρ values. At room temperature, the sensitivity of T1ρ to pH changes had a much higher dynamic range than at body

temperature even in the physiologically relevant pH range. Figure 4.1 below shows the result of the linear regression performed for each relaxation time in the physiologically relevant pH range at 22 °C. The regression shows that T2 and T1ρ are similar in trend because of the large overlap of the confidence bounds, but T1 is different from the two. R^2 values for the T1ρ, T2 and T1 trend-line were 0.965, 0.830 and 0.985 respectively. The confidence bounds were included to show the similarity/difference in the linear models.

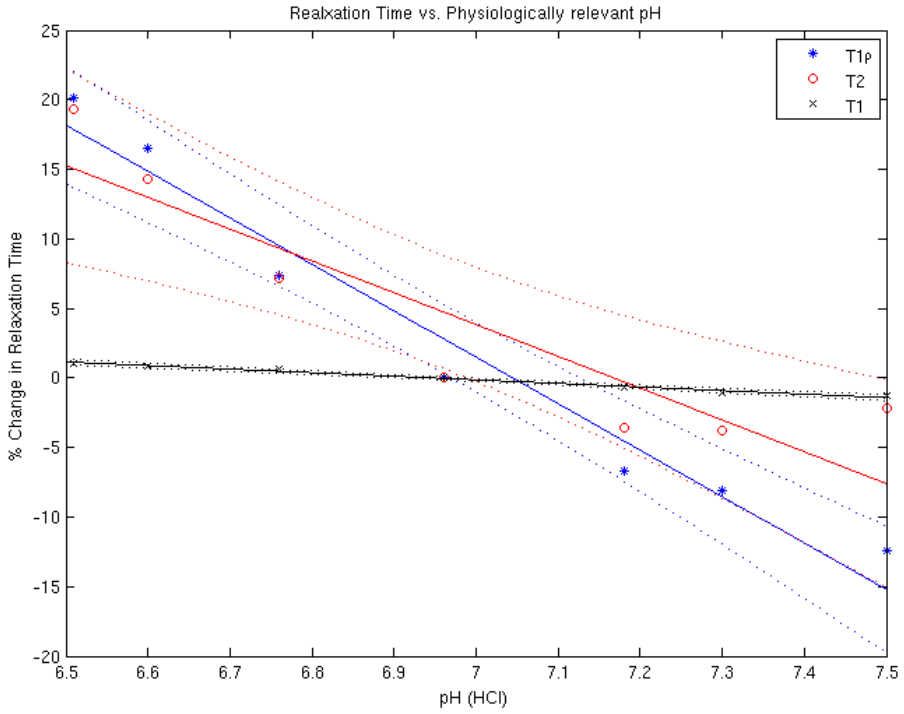

Figure 4.1: Displayed is the linear regression of the percent change plots of T1ρ, T2 and T1 at 22 °C in physiologically relevant pH changes. The blue line is the trend-line for T1ρ, red is for T2 and black for T1 also, the dotted lines in the plot represent the 95% confidence bounds of the regression for each regression.

Aim 2: Determine if T1ρ is more sensitive to glucose changes than T2

The sensitivity of T1ρ to the metabolites glucose was quite low. In the range of glucose concentrations in the human brain (≤ 10mM), T1ρ and T2 change by -0.2% and

0.6% respectively. Also, it seems that viscosity may be the cause of T1ρ and T2 response to the changes in glucose concentration at 3T though viscosity of the imaged solution was not measured. The poor response to glucose concentration changes provided at 3T may be because of the limit on RF power permitted. By calculating the half-width at half-maximum of T1ρ dispersion data collected on a phantom containing glucose, glycogen, and myo-inositol (all of which have hydroxyl groups), Jin *et al*. reported that glucose requires spin-lock frequencies higher than 1kHz to properly distinguish its proton signal from that of water[40]. The specific absorption limits imposed on the clinical scanners and the RF amplifiers provided make it difficult to reach spin-lock frequencies past 1kHz. The experiment used to determine the spin-lock condition was conducted at 9.4T where the chemical shift difference is higher for the detection of the fast exchanging protons of glucose. Relaxation values in small glucose concentrations at 22 °C were fitted to a linear regression model and the results are shown in Figure 4.2. The R^2 value for the T1ρ, T2 and T1 trend lines were 0.748, 0.963 and 0.858 respectively. The confidence bounds plotted as dotted lines show that all three relaxation times are similar in trend because of the large overlap.

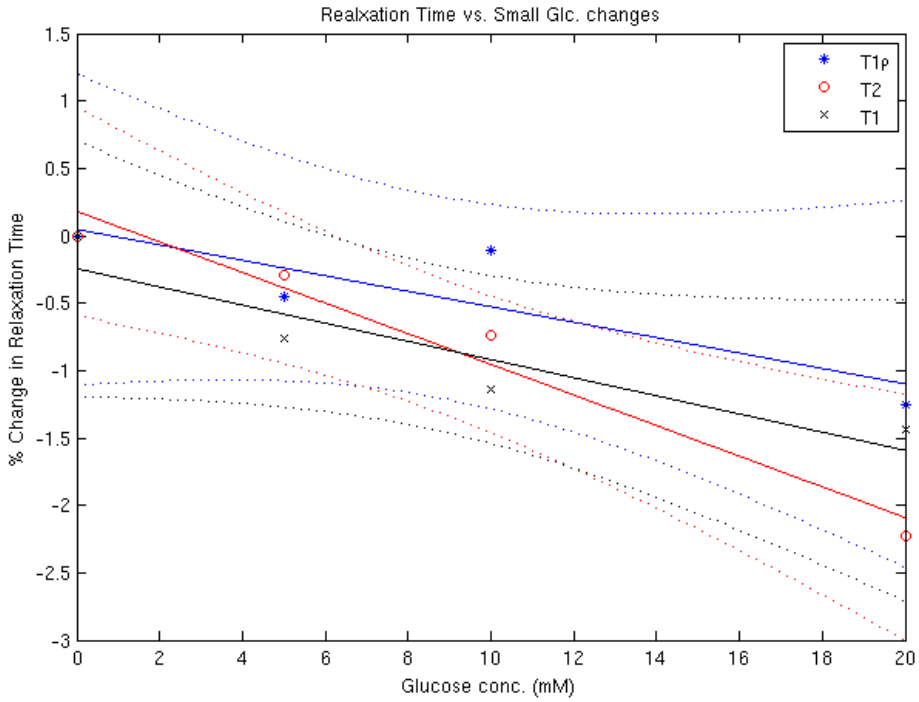

Figure 4.2: Displayed here is the linear regression of the percent change plots of T1ρ, T2 and T1 at 22 °C in small glucose concentration changes. The blue line is the trend-line for T1ρ, red is for T2 and black for T1 also, the dotted lines in the plot represent the 95% confidence bounds of the regression for each regression.

Aim 3: Determine if T1ρ is sensitive to lysine

Lysine, which contains negatively and positively charged structures, was also studied in this work. A carboxyl group (COO^-) provides negative charge and two amino groups (NH_3^+) gives the positive charge. Amide proton exchange provided by the amino group is said to be in the range of 20 – 1200s^{-1}, which extends farther out of the amide proton exchange rates found in peptide bonds of proteins (10-30s^{-1})[15]. Detecting the relaxation of the exchanging lysine protons was thought possible for the lysine experiments at 3T but the exchange rates seem to be faster than can be detected at clinical field strengths. Thus the contribution of charged groups to T1ρ variation could not be determined. If changes in T1ρ due to lysine concentration changes were comparable to that of pH, the experiment that would have been conducted would be to vary pH in constant lysine concentration to determine the effect of hydrogen ion

concentration on the charged structure of lysine. Relaxation values in lysine concentrations at 22 °C were also fitted to a linear regression model and the results are shown in Figure 4.2. The R^2 value for the T1ρ, T2 and T1 trend-lines were 0.953, 0.863 and 0.909 respectively. The confidence bounds plotted with the trend-line show that T1ρ and T2 are similar in trend but T1 is quite different.

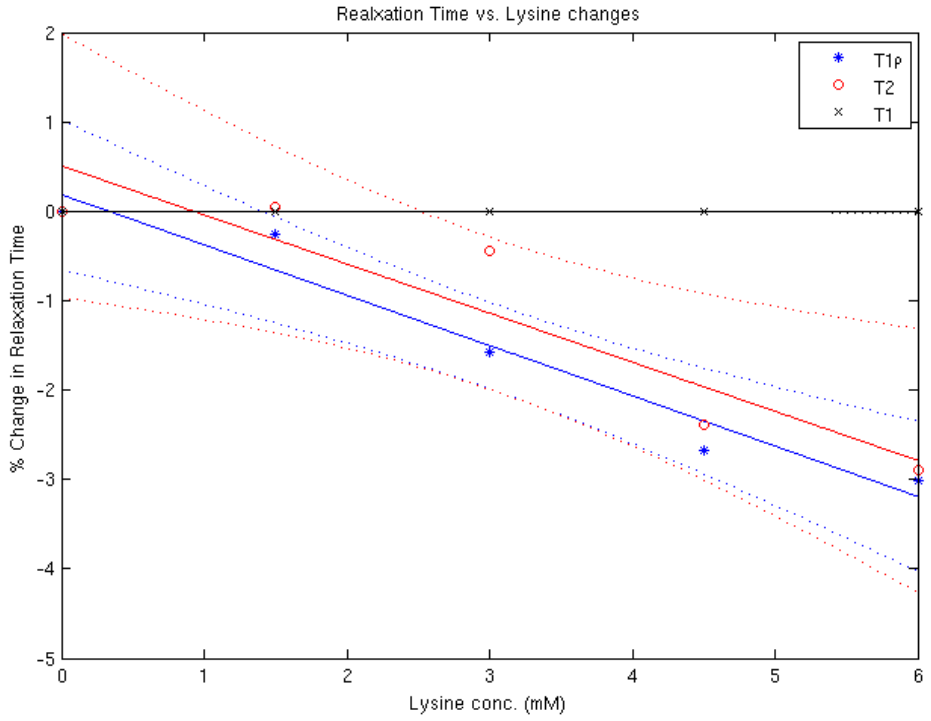

Figure 4.3: Shown here is the difference in the result of the linear regression of the percent change plots of T1ρ, T2 and T1 at 22 °C in lysine concentration changes. The blue line is the trend-line for T1ρ, red is for T2 and black for T1 also, the dotted lines in the plot represent the 95% confidence bounds of the regression for each regression.

Aim 4: Observe relaxation in both pH and metabolite phantoms for a dispersion effect

Dispersion experiments showed frequency dependence on exchange in the pH range of 7.3 to 7.5. This could mean that there is a larger fraction of water molecules bound to solvation layers of proteins or there was more variation in exchange of

proteins in that range of pH values. In the glucose and lysine phantoms, the percent change in relaxation for T1ρ, T2 and T1 were too small to claim frequency dependence for the changes observed. However, the frequency response for the 400Hz frequency dependence was in the same range of percent change as the 20 °C experiments.

In the collection of images for this work, high-resolution scans were performed. The high resolution made the signal more susceptible to noise and thus the error propagation yielded large variations in T1ρ values. This undesired consequence can obscure the line-shape of the changes provide especially if the changes are relatively small. Some of the plots provided in the results do not have error propagation lines drawn because the variations would obscure the lines too much. Homogeneity of the static magnetic field could be a source of noise. In the calculation of median T1ρ changes in selected ROIs, efforts were made to avoid visible effects of B_0 inhomogeneity, however some of these changes may not have been visible.

In conclusion, the characterization of T1ρ was performed using variation of temperature as a factor to determine which metabolite (hydrogen ion, glucose and lysine) would evoke the greatest change in T1ρ values at 3T. Changes in acidity seemed to evoke the greatest change but glucose and lysine did not evoke much change in T1ρ.

FUTURE WORK

It is evident that the pH experiments will have to be repeated multiple times especially at 36 °C. Repeating these experiments will give more statistical significance of the trends being observed. Also, by using the Student's t-test or the ANOVA, differences in the relaxation time can be more clearly stated than with the propagated errors. Having found that T1ρ is more sensitive to physiologically relevant pH changes at 3T, it might prove useful to determine an even narrower range in pH values. The range of pH values could be in from 7.3 to 7.5 since the dispersion data seemed to show the most frequency dependence in that range. The spin-lock frequency could be changed to 800Hz in that range since that frequency evoked the greatest change in that range. With the advent of the 7T magnet at the University of Iowa, it would be interesting to conduct similar relaxation experiments in pH, glucose and lysine phantoms to see how the results compare the results of 3T.

REFERENCES

1. Paulsen, J. S. *et al.* Detection of Huntington's disease decades before diagnosis: the Predict-HD study. *J. Neurol. Neurosurg. Psychiatry* **79,** 874–880 (2008).

2. Berk, M. *et al.* Pathways underlying neuroprogression in bipolar disorder: Focus on inflammation, oxidative stress and neurotrophic factors. *Neurosci. Biobehav. Rev.* **35,** 804–817 (2011).

3. Aquilani, R. *et al.* Is stroke rehabilitation a metabolic problem? *Brain Inj.* **28,** 161–173 (2014).

4. Ball, S. & Shekhar, A. Basilar artery response to hyperventilation in panic disorder. *Am. J. Psychiatry* **154,** 1603–1604 (1997).

5. Choi, N. C. *et al.* Dose-response relationship between probability of pathologic tumor control and glucose metabolic rate measured with FDG PET after preoperative chemoradiotherapy in locally advanced non-small-cell lung cancer. *Int. J. Radiat. Oncol.* **54,** 1024–1035 (2002).

6. Gillies, R. J., Raghunand, N., Garcia-Martin, M. L. & Gatenby, R. A. pH imaging. A review of pH measurement methods and applications in cancers. *IEEE Eng. Med. Biol. Mag. Q. Mag. Eng. Med. Biol. Soc.* **23,** 57–64 (2004).

7. Kemp, G. J. Non-invasive methods for studying brain energy metabolism: what they show and what it means. *Dev. Neurosci.* **22,** 418–428 (2000).

8. Duncan, J. S. Magnetic resonance spectroscopy. *Epilepsia* **37,** 598–605 (1996).

9. Heo, H.-Y., Wemmie, J., Thedens, D. & Magnotta, V. A. Evaluation of activity-dependent functional pH and T1ρ response in the visual cortex. *NeuroImage* **95,** 336–343 (2014).

10. Magnotta, V. A. *et al.* Detecting activity-evoked pH changes in human brain. *Proc. Natl. Acad. Sci. U. S. A.* **109,** 8270–8273 (2012).

11. Clarke, J. L. & Chang, S. M. Neuroimaging: diagnosis and response assessment in glioblastoma. *Cancer J. Sudbury Mass* **18,** 26–31 (2012).

12. Haris, M. *et al.* Early marker for Alzheimer's disease: hippocampus T1rho (T(1rho)) estimation. *J. Magn. Reson. Imaging JMRI* **29,** 1008–1012 (2009).

13. Borthakur, A. *et al.* Sodium and T1rho MRI for molecular and diagnostic imaging of articular cartilage. *NMR Biomed.* **19,** 781–821 (2006).

14. Zaiss, M. & Bachert, P. Chemical exchange saturation transfer (CEST) and MR Z-spectroscopy in vivo: a review of theoretical approaches and methods. *Phys. Med. Biol.* **58,** R221 (2013).

15. Van Zijl, P. C. M. & Yadav, N. N. Chemical exchange saturation transfer (CEST): what is in a name and what isn't? *Magn. Reson. Med. Off. J. Soc. Magn. Reson. Med. Soc. Magn. Reson. Med.* **65,** 927–948 (2011).

16. Kogan, F., Hariharan, H. & Reddy, R. Chemical Exchange Saturation Transfer (CEST) Imaging: Description of Technique and Potential Clinical Applications. *Curr. Radiol. Rep.* **1,** 102–114 (2013).

17. Togao, O. *et al.* Characterization of Lung Cancer by Amide Proton Transfer (APT) Imaging: An In-Vivo Study in an Orthotopic Mouse Model. *PLoS ONE* **8,** e77019 (2013).

18. Sagiyama, K. *et al.* In vivo chemical exchange saturation transfer imaging allows early detection of a therapeutic response in glioblastoma. *Proc. Natl. Acad. Sci. U. S. A.* **111,** 4542–4547 (2014).

19. Haris, M. *et al.* MICEST: a potential tool for non-invasive detection of molecular changes in Alzheimer's disease. *J. Neurosci. Methods* **212,** 87–93 (2013).

20. Kogan, F. *et al.* In vivo chemical exchange saturation transfer imaging of creatine (CrCEST) in skeletal muscle at 3T. *J. Magn. Reson. Imaging JMRI* **40,** 596–602 (2014).

21. Sepponen, R. E., Pohjonen, J. A., Sipponen, J. T. & Tanttu, J. I. A method for T1 rho imaging. *J. Comput. Assist. Tomogr.* **9,** 1007–1011 (1985).

22. Johnson, C. P. *et al.* Brain abnormalities in bipolar disorder detected by quantitative T1ρ mapping. *Mol. Psychiatry* (2015). doi:10.1038/mp.2014.157

23. Wassef, S. N. *et al.* T1ρ imaging in premanifest Huntington disease reveals changes associated with disease progression. *Mov. Disord. Off. J. Mov. Disord. Soc.* (2015). doi:10.1002/mds.26203

24. Haris, M. *et al.* T1rho (T1ρ) MR imaging in Alzheimer' disease and Parkinson's disease with and without dementia. *J. Neurol.* **258,** 380–385 (2010).

25. Duvvuri, U. *et al.* Quantitative T1rho magnetic resonance imaging of RIF-1 tumors in vivo: detection of early response to cyclophosphamide therapy. *Cancer Res.* **61,** 7747–7753 (2001).

26. Immonen, R., Kharatishvili, I., Gröhn, O. & Pitkänen, A. MRI biomarkers for post-traumatic epileptogenesis. *J. Neurotrauma* **30,** 1305–1309 (2013).

27. Pan, J. W., Hamm, J. R., Rothman, D. L. & Shulman, R. G. Intracellular pH in human skeletal muscle by 1H NMR. *Proc. Natl. Acad. Sci. U. S. A.* **85,** 7836–7839 (1988).

28. Hulvershorn, J. *et al.* T1rho contrast in functional magnetic resonance imaging. *Magn. Reson. Med.* **54,** 1155–1162 (2005).

29. Johnson, C. P., Heo, H.-Y., Thedens, D. R., Wemmie, J. A. & Magnotta, V. A. Rapid acquisition strategy for functional T1ρ mapping of the brain. *Magn. Reson. Imaging* **32,** 1067–1077 (2014).

30. Jin, T. & Kim, S.-G. Characterization of non-hemodynamic functional signal measured by spin-lock fMRI. *NeuroImage* **78,** 385–395 (2013).

31. Magnotta, V. A., Johnson, C. P., Follmer, R. & Wemmie, J. A. Functional t1ρ imaging in panic disorder. *Biol. Psychiatry* **75,** 884–891 (2014).

32. Baum, J., Tycko, R. & Pines, A. Broadband and adiabatic inversion of a two-level system by phase-modulated pulses. *Phys. Rev. A* **32,** 3435–3447 (1985).

33. Balchandani, P., Pauly, J. & Spielman, D. Designing adiabatic radio frequency pulses using the Shinnar-Le Roux algorithm. *Magn. Reson. Med.* **64,** 843–851 (2010).

34. Pauly, J., Le Roux, P., Nishimura, D. & Macovski, A. Parameter relations for the Shinnar-Le Roux selective excitation pulse design algorithm [NMR imaging]. *IEEE Trans. Med. Imaging* **10,** 53–65 (1991).

35. Grösch, L. & Noack, F. NMR relaxation investigation of water mobility in aqueous bovine serum albumin solutions. *Biochim. Biophys. Acta BBA - Protein Struct.* **453,** 218–232 (1976).

36. Sheinblatt, M. Nuclear Magnetic Resonance Study of the Protolysis Kinetics of the Peptide Hydrogens of Triglycine1a. *J. Am. Chem. Soc.* **88,** 2123–2126 (1966).

37. Engelhardt, R. T. & Johnson, G. A. T1ρ relaxation and its application to MR histology. *Magn. Reson. Med.* **35,** 781–786 (1996).

38. De Crespigny, A. J., Wendland, M. F., Derugin, N., Kozniewska, E. & Moseley, M. E. Real-time observation of transient focal ischemia and hyperemia in cat brain. *Magn. Reson. Med.* **27,** 391–397 (1992).

39. Kettunen, M. I., Gröhn, O. H. J., Silvennoinen, M. J., Penttonen, M. & Kauppinen, R. A. Effects of intracellular pH, blood, and tissue oxygen tension on T1rho relaxation in rat brain. *Magn. Reson. Med.* **48,** 470–477 (2002).

40. Jin, T., Mehrens, H., Hendrich, K. S. & Kim, S.-G. Mapping brain glucose uptake with chemical exchange-sensitive spin-lock magnetic resonance imaging. *J. Cereb. Blood Flow Metab. Off. J. Int. Soc. Cereb. Blood Flow Metab.* **34,** 1402–1410 (2014).

41. Zu, Z., Spear, J., Li, H., Xu, J. & Gore, J. C. Measurement of regional cerebral glucose uptake by magnetic resonance spin-lock imaging. *Magn. Reson. Imaging* **32,** 1078–1084 (2014).

42. Kettunen, M. I., Gröhn, O. H., Penttonen, M. & Kauppinen, R. A. Cerebral T1rho relaxation time increases immediately upon global ischemia in the rat independently of blood glucose and anoxic depolarization. *Magn. Reson. Med.* **46,** 565–572 (2001).